



THE
UNIVERSITY
OF
ILLINOIS
AT
CHICAGO

4

AD-A211 372

Laboratory for Atomic, Molecular, and Radiation Physics (M/C 273)
Department of Physics
College of Liberal Arts and Sciences
Box 4348, Chicago, Illinois 60680
(312) 996-4868

6 July 1989

PROGRESS REPORT

LASER PRODUCTION OF SOFT X-RAYS BY MULTIQUANTUM PROCESSES
AND THE EXCITATION OF ATOMIC INNER-SHELL STATES

Contract Report:	N00014-87-K-0558
Principal Investigator:	Charles K. Rhodes
Co-Investigators:	Ting Shan Luk Armon McPherson Keith Boyer
Prepared for:	Dr. Herschel S. Pilloff Office of Naval Research Code 1112LO, Physics Branch 800 North Quincy Street Arlington, VA 22217

DTIC
ELECTE
AUG 04 1989
S B D
MB

DISTRIBUTION STATEMENT A

Approved for public release;
Distribution Unlimited

89 7 25 041

Table of Contents

ABSTRACT	ii
I. INTRODUCTION	1
II. DISCUSSION OF RESEARCH	2
A. High Intensity Subpicosecond Ultraviolet Light Source	2
B. Preliminary Studies of Molecular Excitation Exhibiting Direct Multiquantum $2\sigma_g$ Hole Generation in N_2	3
1. Ion Studies of N_2	3
2. Fluorescence Studies of N_2	4
a. Overall Character of 55.8-nm Emission	5
b. Consideration of the Molecular Charge State	9
c. Analysis of the Specific Levels	12
d. Analysis of the Transition	15
C. Consideration of the Multiquantum Strong-Field Mode of Excitation .	19
1. Inner-Electron Excitation	19
2. General Features of Strong-Field Coupling	21
III. CONCLUSIONS	32
IV. REFERENCES	33
V. APPENDICES	36
Appendix A: "Ultrahigh Intensity KrF* Laser System"	36
Appendix B: "Kinetic Energy Distributions of Ionic Fragments Produced by Subpicosecond Multiphoton Ionization of N_2 "	49

Accession For	
NTIS GRA&I	<input checked="" type="checkbox"/>
DTIC TAB	<input type="checkbox"/>
Unannounced	<input type="checkbox"/>
Justification	
By <i>per letter</i>	
Distribution/	
Availability Codes	
Dist	Avail and/or Special
A-1	



ABSTRACT

Atomic and molecular materials exhibit complex behavior when exposed to strong externally applied fields. A research program, whose goal is the understanding of the nonlinear processes governing the coupling of intense radiation to atomic and molecular matter, is currently underway at the University of Illinois at Chicago. The general amplitude under study is $NY + X \rightarrow X^{q*} + qe^- + \gamma'$, a class of processes which involves ionization with the collateral production of energetic electrons and radiation. Recently developed ultraviolet light sources are enabling the attainment of focal intensities such that the strong-field regime ($\epsilon \gg e/a_0^2$) can now be systematically studied. This is a completely unexplored regime of interaction experimentally and one in which current theoretical descriptions provide little guidance. It was anticipated that such conditions would produce unusual excited states of matter and that expectation has been confirmed by recent experimental findings revealing the direct multiphoton production of inner-orbital ($2\sigma_g^{-1}$) excited states of N_2^+ and N_2^{2+} . Indeed, it can be shown that the strong-field coupling represents a unique mode of interaction which combines (1) the application of strong electromagnetic forces with (2) a very small collateral transfer of energy. This regime is impossible to achieve with charged particle collisions or with low intensity radiation of any frequency. Interactions of this type are particularly effective in exciting electronic motions along specific molecular axes enabling the generation of new forms of highly excited matter regardless of molecular structure or composition.

I. INTRODUCTION

The response of atomic and molecular materials to intense short-pulse radiation is an active area of inquiry. A subject of marked interest, in which multiquantum and strong-field processes can play a significant role, concerns the mechanisms leading to the production of electronically excited states, particularly inner-shell excitations which radiate in the x-ray region. Roughly speaking, we are interested in the physical regime involving intensities $\gtrsim 10^{18}$ W/cm² so that the peak field strength ϵ is significantly above an atomic unit (e/a_0^2). The experimental picture,¹ as outlined in Appendix A, is now such that this regime can be systematically studied and this document proposes a program of research whose goal is the understanding of these strong-field phenomena.

It has been suggested²⁻⁵ that, for sufficiently strong coupling, fundamentally different nonlinear modes of direct electronic excitation may occur. The experimental results of two recent studies, one involving ion production⁶ and the other concerning fluorescence,⁷ have produced strong confirming evidence for this hypothesis with the unambiguous observation of the direct generation of $2\sigma_g$ holes in N_2 . The ion studies are described in Appendix B and important new findings stemming from the analysis of the fluorescence spectra of N_2 are discussed below in Section II.B. Indeed, the main conclusions that emerge from the consideration of these results is (1) that inner electrons can be directly excited and (2) that the strong-field coupling is qualitatively different from those that can be generated by other forms of interaction, particularly charged particle collisions, even though the force field can be of comparable peak strength in the collisional case. Consequently, the strong-field interaction characterizes a unique regime of molecular interaction enabling the efficient production of new forms of highly excited atomic and molecular matter.

II. DISCUSSION OF RESEARCH

A. High Intensity Subpicosecond Ultraviolet Light Source

The capabilities of the light source which we are now using in our research are described in Appendix A. These results definitively show that a focal intensity of $\sim 2 \times 10^{19}$ W/cm² is now achievable, a value corresponding to an electric field amplitude ϵ of $\sim 24 (e/a_0^2) \approx 1.2 \times 10^{11}$ V/cm. This intensity, which is approximately one thousand-fold greater than that characteristic of all our previous work, clearly opens up a new regime of interaction and permits, for the first time, the systematic study of processes for which $\epsilon \gg e/a_0^2$. As an instrument for use in the study of strong-field phenomena, this source is unique world-wide. The present capability of the source enables the generation of a maximum intensity $I \approx 2 \times 10^{19}$ W/cm², a value only slightly below the Compton intensity⁸⁻¹⁰ ($I_{Co} \approx 4.5 \times 10^{19}$ W/cm²) at 248-nm.

It is also important to realize that this light source is not operating at the limit of its potential and that relatively straight-forward improvements can significantly increase the maximum focal intensity. Two steps are planned to increase the available intensity. They are (1) the use of shorter pulses^{11,12} (~ 100 fs) in the amplifier chain and (2) the optimization of the large aperture (100 cm²) power amplifier to further increase the pulse energy.

We now compare the measured parameters of the currently operating system with the limiting values that we feel the system can attain with suitable optimization. This comparison is given in Table I. In terms of the maximum electric field, or equivalently, the force that can be exerted on a charged particle, the present system is within a factor of ~ 7.5 of the limiting value believed to apply for this instrument. The pulse width of ~ 600 fs has been broadened to some extent by the effect of group velocity dispersion arising from the optical elements associated

with the large aperture power amplifier. This pulse broadening effect can be eliminated by known techniques¹³⁻¹⁵ using either prisms or gratings. In addition, shorter pulses can be generated with a modified source for the production of the seed beam. Certain mechanical and electrical changes in the power amplifier are also indicated which will raise the output energy. The resources required to implement these improvements have been requested from another agency.

TABLE I
Comparison of Current and Projected Operating
Parameters for the 248-nm System

Parameter	Current Measured Value	Projected Developed Value
Pulse Energy (J)	~ 0.350	1.0
Pulse Width (fs)	~ 600	100
Focal Spot Diameter (μm)	$\gtrsim 1.7$	1.0 - 1.2
Maximum Intensity (W/cm^2)	2.0×10^{19}	$\sim 10^{21}$
Maximum Electric Field (V/cm)	$\sim 1.2 \times 10^{11}$	$\sim 9 \times 10^{11}$
Pulse Repetition Rate (s^{-1})	0.5	1.0

B. Preliminary Studies of Molecular Excitation Exhibiting Direct Multiquantum $2\sigma_g$ Hole Generation in N_2

1. Ion Studies of N_2

Experimental results now exist which clearly show the excitation of inner electrons by a direct multiquantum process. The specific system illustrating this process is N_2 in which the production of $2\sigma_g$ holes has been detected in two different experimental studies. The initial hint, as described in Appendix B, came

from the measurement⁶ of kinetic energy distributions of ionic fragments produced in N_2 which indicated the presence of the charge asymmetric channel



resulting from multiphoton ionization. Since other experiments¹⁶ examining soft x-ray produced fragmentation of N_2 showed that process (1) corresponds to the production of a two-hole state having an excitation energy of ~ 70 eV, the obvious implication was that the laser excitation produced a similar configuration of molecular excitation. The states^{17,18} implicated in the x-ray studies¹⁶ of N_2 , which has the ground state configuration $(1\sigma_g)^2(1\sigma_u)^2(2\sigma_g)^2(2\sigma_u)^2(1\pi_u)^4(3\sigma_g)^2$, were $^1\Sigma_g[2\sigma_g^{-1}, 3\sigma_g^{-1}]$, $^1\Sigma_u[2\sigma_g^{-1}, 2\sigma_u^{-1}]$, and $^1\Pi_u[2\sigma_g^{-1}, 1\pi_u^{-1}]$, all involving a $2\sigma_g$ hole. We note that the $2\sigma_g$ orbital has a binding energy of 37.7 eV, a value considerably higher than the $2\sigma_u$ (18.7eV), $1\pi_u$ (15.6 eV), and $3\sigma_g$ (16.7eV) orbitals. Therefore, the N_2^{2+} states having a $2\sigma_g$ vacancy and correlating to the $N^{2+} + N$ asymptote have an energy substantially above the lowest manifold of states¹⁹ in N_2^{2+} which are associated with the $N^+ + N^+$ limit. Furthermore, it has been noted²⁰ that the $2\sigma_g$ hole is a highly correlated state and does not fit a quasi-particle picture. This makes states with $2\sigma_g$ holes of particular interest in studies of multiphoton coupling.

2. Fluorescence Studies of N_2

The preliminary measurements of fluorescence discussed below point toward new insights into the mechanisms of multiphoton excitation. We describe below the observation of a very intense band of radiation at ~ 55.8 nm which appears to be directly related to the mode of excitation producing the charge asymmetric fragmentation represented by process (1). The 55.8-nm emission is, at the outset, highly unusual in one obvious respect. Although the spectrum of N_2 has been studied for nearly a century¹⁸ with many techniques of excitation, we have been

unable to find any previous^{18,21} report of such a characteristic emission originating from material composed solely of nitrogen atoms or molecules in either neutral or ionic form. From this fact alone, it appears that the observation of the 55.8 nm band originates from the excitation of a new class of states and that the strong production of these levels is intimately connected with the basic nature of the multiquantum mechanism involved in the coupling to the molecule. This line of reasoning and its implications are explored in the following discussion.

The fluorescence spectra observed in these studies have been recorded in the 7 – 79 nm range using an experimental configuration previously described.²² The spectral resolution of the spectrometer–detector system is slightly less than 0.1 nm FWHM. Typical target gas densities, produced with a pulsed valve, ranged from 10^{16} – 6×10^{19} cm⁻³. The source used for excitation is the subpicosecond (~ 600 fs) KrF* (248 nm) system described in Appendix A. The peak intensities produced by the focusing lens used in these preliminary experiments were estimated to be in the 10^{16} – 10^{17} W/cm² range, a value which corresponds to a field strength on the order of one atomic unit (e/a_0^2).

a. Overall Character of 55.8-nm Emission

A section of the N₂ spectrum exhibiting the anomalous 55.8-nm feature is shown in Fig. (1). The spectrum in this range has several salient characteristics: (1) a characteristic frequency that does not match any known transition arising from an atomic,²³ molecular,¹⁸ or ionic²³ species; (2) an anomalously large linewidth (~ 0.3 nm FWHM); and (3) an integrated intensity comparable to the strongest lines observed throughout the entire spectral region (7 – 79 nm) studied. Since research grade N₂ was used, the 55.8-nm line could not reasonably be associated with impurities.

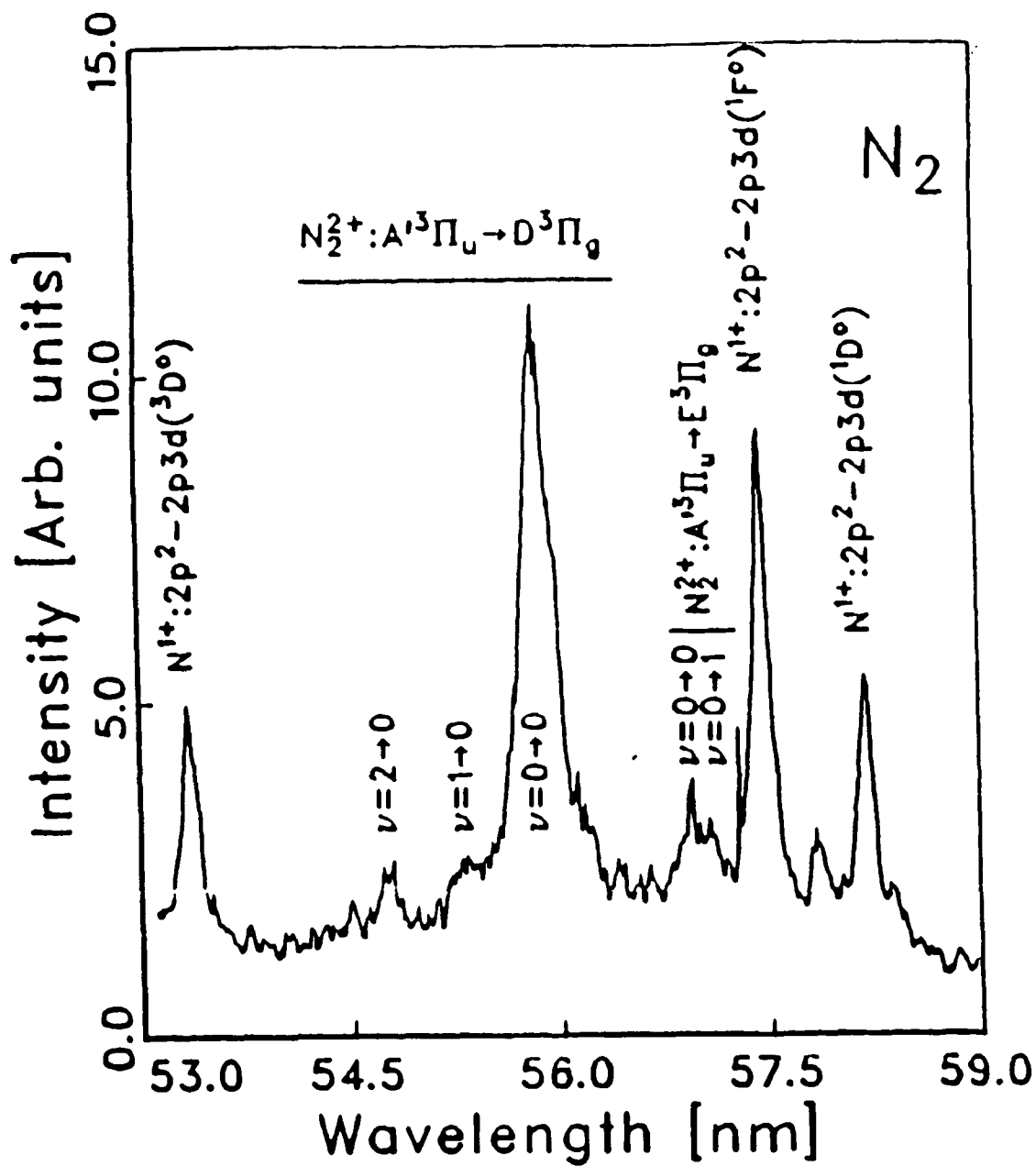


Fig. (1): The spectrum observed in N_2 in the 56-nm region produced with intense subpicosecond (~ 600 fs) 248-nm irradiation. Two groups of molecular features are identified, including the main transition at 55.8-nm, as well as several atomic lines. The density of N_2 used was $\sim 10^{19} \text{ cm}^{-3}$.

At the intensities used in this experiment, the irradiation of N_2 produces abundant quantities of atomic nitrogen ions which, subsequently, can be excited through collisional processes in the resulting plasma. If the 55.8-nm feature were generated by collisional excitation and/or recombination producing an excited atomic nitrogen atom or ion, the line would arise naturally from the irradiation of any molecule containing substantial quantities of nitrogen. Conversely, if the excited state production depended specifically upon the irradiation of N_2 , other substances would be ineffective in producing the anomalous band or, perhaps, lead to a modified appearance depending upon the molecular structure. In order to evaluate this molecular dependence, the experiment was repeated with N_2O . This was done for the same range of target gas density so that both the heavy body and resulting electron densities would be comparable in both cases.

The spectrum observed around 56 nm in N_2O , for the same conditions of irradiation as those used for N_2 , is shown in Fig. (2). In comparison to Fig. (1), the important features are: (1) the total lack of the 55.8-nm feature in the N_2O spectrum; (2) the clear presence of a known $N^+ 2p^2 - 2p3d (^1F^o)$ (57.4 nm) line in both the N_2 and N_2O data; and (3) the additional presence of several atomic oxygen ion (O^+ , O^{3+}) lines in the N_2O spectrum. Furthermore, throughout the entire spectral region studied, many of the atomic nitrogen ion lines seen in N_2 , such as the N^{++} Li-like transitions,^{23,24} are also observed in N_2O . These observations support the conclusion that, while much of the atomic ion radiation may result from plasma processes, the 55.8-nm radiation does not.

The clear implications of the comparison between N_2 and N_2O are: (1) that the direct irradiation of N_2 is required to produce the 55.8-nm fluorescence, and (2) that the excited state production is sensitive to the details of the molecular structure.

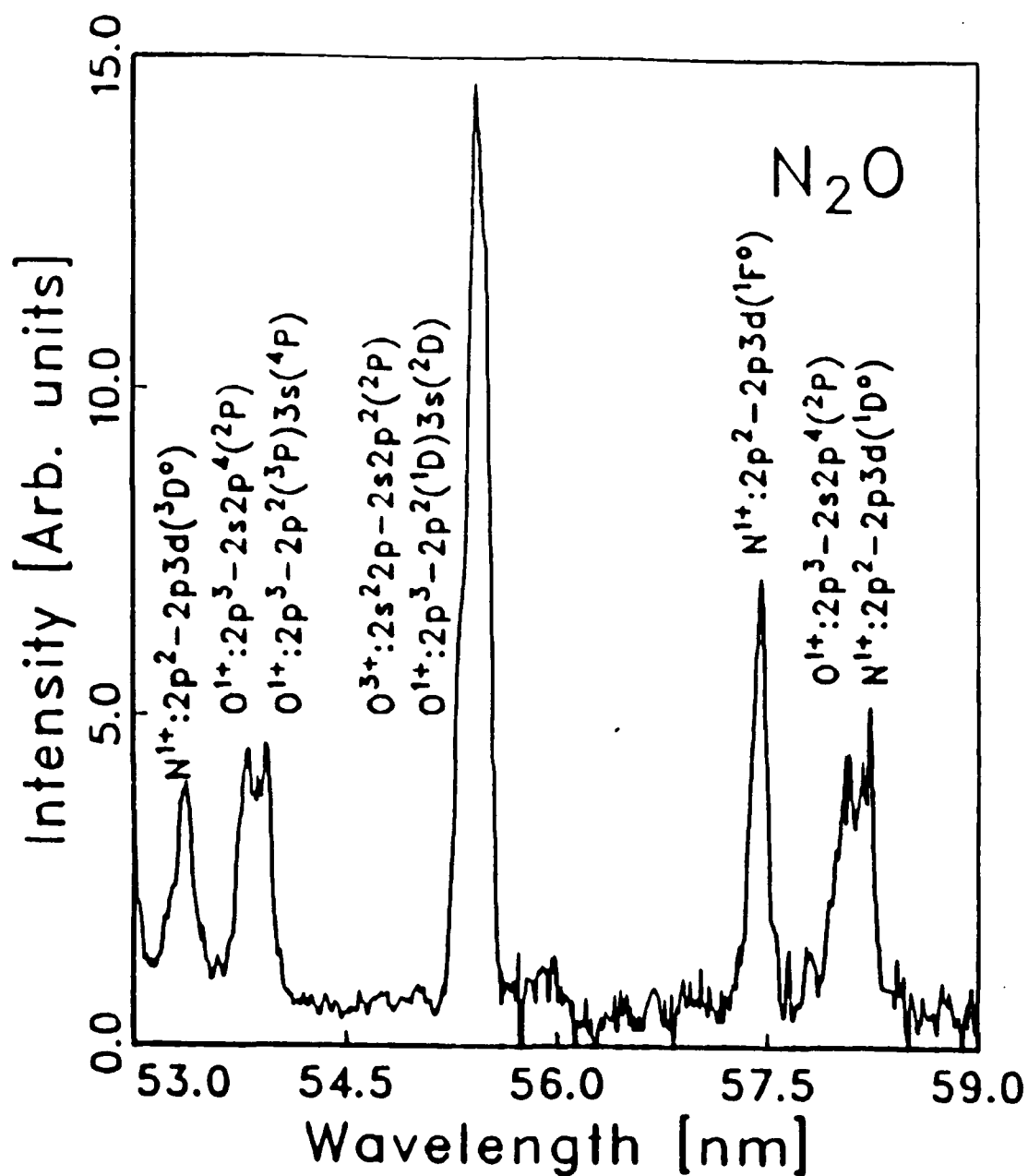


Fig. (2): The spectrum observed in N_2O in the 56-nm region for conditions of irradiation identical to those corresponding to the data shown in Fig. (1). Several atomic nitrogen and oxygen lines are identified with the dominant feature produced by O^{1+} and O^{3+} . The density of N_2O used was $\sim 10^{19} \text{ cm}^{-3}$.

In addition to the prominent 55.8-nm transition, eight weaker but distinct and previously unidentified lines were also seen in N_2 , but not in N_2O . The natural implication is that they are of similar origin. Although the remainder of this discussion is mainly devoted to determining the molecular charge state and levels producing the 55.8-nm line, mention will be made of these other anomalous transitions in order to support the physical picture motivated by these findings.

b. Consideration of the Molecular Charge State

A partial diagram of the potential energy curves for N_2 , illustrating the specific states referred to in this section, is shown in Fig. (3). The neutral N_2 molecule can be ruled out immediately as a source of the 55.8-nm radiation. Since the observed radiation corresponds to a transition energy of 22.2 eV and since N_2 has an ionization potential of 15.6 eV, it is expected that autoionization would effectively damp such a transition.

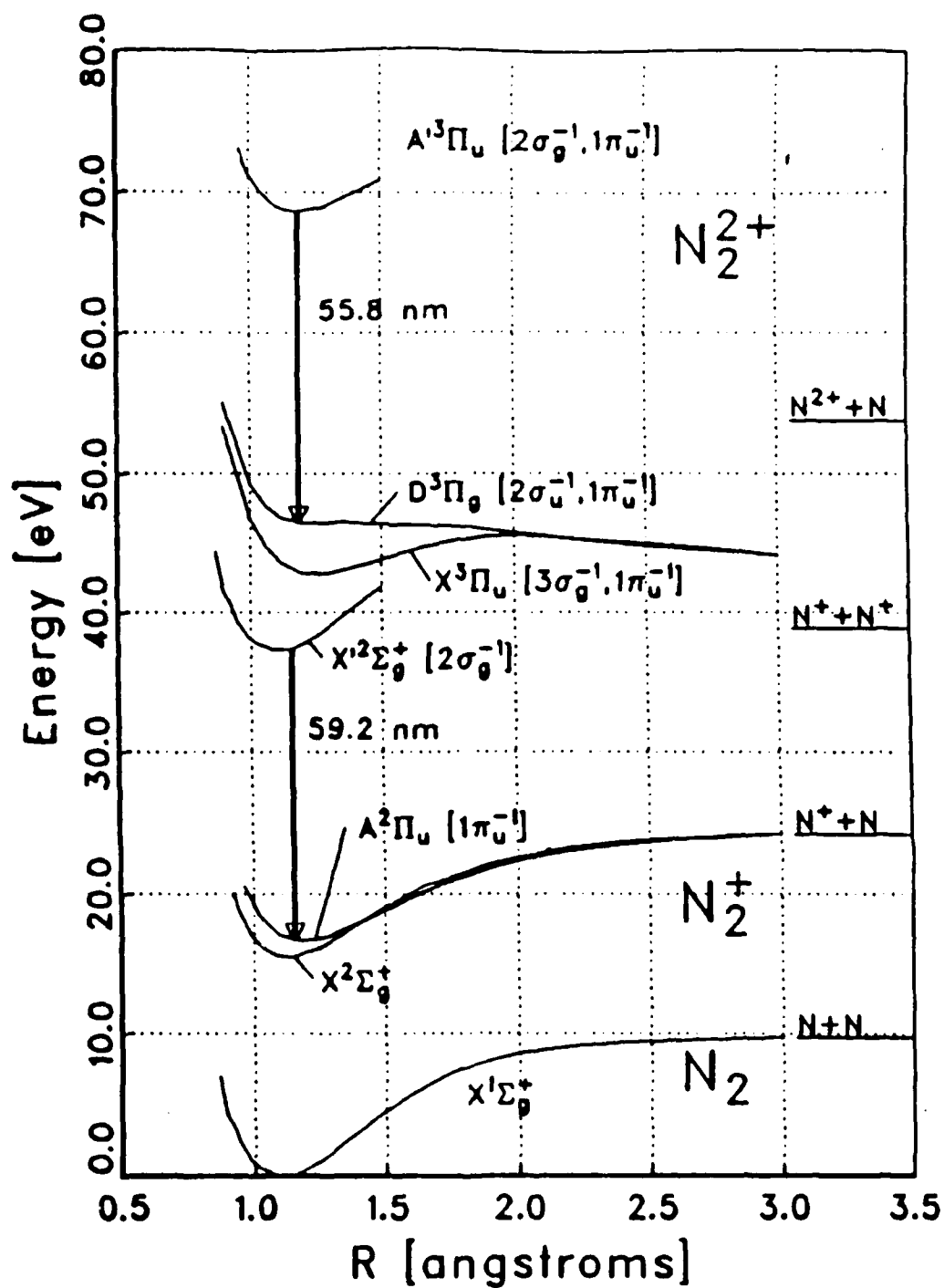


Fig. (3): Potential energy curves for N_2 for selected states of interest. Two observed transitions involving a $2\sigma_g$ hole are indicated. Data for the curves were taken from a variety of sources [Ref. (17), Ref. (18), and Ref. (19)] as well as the authors' own estimates. Dissociation limits are given for reference.

Based on the spectroscopy of N_2 and N_2^+ , the binding energies associated with the $1\pi_u$, $3\sigma_g$, $2\sigma_u$, and $2\sigma_g$ orbitals are 15.6 eV, 16.7 eV, 18.7 eV, and 37.7 eV, respectively.²⁵ Thus, the removal of a $2\sigma_g$ electron would be required to produce a state in N_2^+ capable of emitting the 55.8-nm radiation. In fact, the difference between the binding energy of the $2\sigma_g$ orbital and the energy of the lowest level in N_2^+ (~ 15.6 eV) is quite close to the energy of the observed radiation. Since the ionization potential of N_2^+ is ~ 27 eV, a state involving a $2\sigma_g$ hole at 22.2 eV above the N_2^+ ground state would not autoionize and appears, at least energetically, to be a possible origin of the 55.8-nm emission. However, a configuration having a single excitation comprised of a $2\sigma_g$ hole is of gerade symmetry and since the ground state of N_2^+ is $X^2\Sigma_g^+$, the symmetries of these configurations strictly forbid a dipole transition between them. However, we observe that the first excited state of N_2^+ is $A^2\Pi_u$ and, therefore, could be a dipole allowed lower level. While this could not explain the 55.8-nm emission, the wavelength of a transition terminating on the $A^2\Pi_u$ state would be at ~ 59.3 nm and, in fact, a weak unidentified line is observed close to this value, at 59.2 nm in N_2 , but not in N_2O . Consequently, this radiation presumably arises from a $^2\Sigma_g$ state in N_2^+ involving a $2\sigma_g$ hole, hereafter referred to as $X'^2\Sigma_g$. Thus, while excited N_2^+ appears to be produced, a clear identification could not be made from this charge state for the dominant 55.8-nm band.

The limitations involving an assignment of the 55.8-nm feature to the N_2^+ system vanish if N_2^{2+} is considered. Extensive calculations¹⁹ exist on the properties of low lying N_2^{2+} levels around 45 eV and less complete results for the levels involving a $2\sigma_g$ hole at higher energies are also available.¹⁷ As determined in the synchrotron studies,¹⁶ these upper levels cluster in the vicinity of 70 eV and, therefore, have an energy scale sufficient for a transition of ~ 22 eV. Furthermore,

states of all symmetries exist in these two energy bands so that opportunities for transitions obeying normal dipole selection rules exist. Finally, since N_2^{3+} and higher charge states of the molecule do not support any bound levels, N_2^{2+} emerges as the most natural and, indeed, only candidate for the observed transition.

c. Analysis of the Specific Levels

Previous work⁶ on multiphoton ionization of N_2 indicated that at least some of the upper levels in N_2^{2+} having a $2\sigma_g$ hole are produced directly by a multiphoton process. Although many of these states are possible candidates for the upper level of the 55.8-nm transition, most can be eliminated. Auger-electron/ion coincidence studies¹⁶ of N_2 show that all of the $2\sigma_g$ hole states in the 70-eV energy range produced through KLL Auger processes dissociate rapidly into $N^{2+} + N$. Thus, all the states in this region observed in Auger work would be expected to have a very low radiative yield. In addition, the observed line has a large width which, as argued below, appears to rule out a single-to-single transition, assuming that the transition is bound-bound. Of the $2\sigma_g$ hole states calculated in Ref. (17), there is only one triplet state in the correct energy range which has not been identified from Auger work: the $^3\Pi_u$ state with a dominant electronic configuration $(2\sigma_g^{-1}, 1\pi_u^{-1})$, hereafter designated $A'^3\Pi_u$. Selection rules would then require a lower level with triplet gerade symmetry.

Calculations¹⁹ of the lower levels of N_2^{2+} , which correlate to the $N^+ + N^+$ asymptote, show the existence of several states having the correct symmetry to be the lower state of the 55.8-nm transition. With the upper state identified, the observed transition energy can be used to distinguish among these possible lower levels. The energy scales of Ref. (17) and Ref. (19) are reconciled by matching the energy of the $a^1\Sigma_g^+$ level, which, in Ref. (19), is found to be 42.9 eV above the N_2 ground state. This places the upper state of the 55.8-nm transition at an

energy of 68.5 eV and the lower state at a corresponding value of 46.3 eV. The $D^3\Pi_g$ state of N_2^{2+} , the lowest of that symmetry with an electronic configuration $(2\sigma_u^{-1}, 1\pi_u^{-1})$, is calculated¹⁹ to be at 46.44 eV, and thus, is determined to be the lower level of the 55.8-nm transition. Independent calculations²⁰ of these states give a transition energy of 21.9 eV, a value in quite close agreement with the above results.

Other dipole-allowed lower states exist, such as the $A^3\Sigma_g^-$, $E^3\Pi_g$, and $G^3\Pi_g$. While these cannot be the lower level of the 55.8-nm feature, it is possible to associate several of the weaker and otherwise unidentified lines uniquely observed in N_2 to transitions involving these states. These assignments are presented in Table II. It is interesting to note that one of the transitions in Table II, referred to above in Section II.B.2.b, involves N_2^+ , a case which implies that the $2\sigma_g$ electron is removed without the additional loss of any valence electrons.

TABLE II

Assignment of Observed Transitions to
States of Molecular Nitrogen Ions

Observed Wavelength (nm)	Energy (eV)	Identification*	Vibrational* Levels ($\nu - \nu'$)	Electronic Configuration**
67.57	18.35	$N_2^{2+}: A' \ ^3\Pi_U \rightarrow G \ ^3\Pi_g$	0 - 1	$2\sigma_g^{-1} 1\pi_U^{-1} - 2\sigma_U^{-1} 1\pi_U^{-1}$
59.15	20.96	$N_2^{1+}: X' \ ^2\Sigma_g \rightarrow A \ ^2\Pi_U$	0 - 0	$2\sigma_g^{-1} - 1\pi_U^{-1}$
57.16	21.69	$N_2^{2+}: A' \ ^3\Pi_U \rightarrow E \ ^3\Pi_g$	0 - 1	$2\sigma_g^{-1} 1\pi_U^{-1} - 2\sigma_U^{-1} 1\pi_U^{-1}$
57.02	21.74	$N_2^{2+}: A' \ ^3\Pi_U \rightarrow E \ ^3\Pi_g$	0 - 0	$2\sigma_g^{-1} 1\pi_U^{-1} - 2\sigma_U^{-1} 1\pi_U^{-1}$
55.84	22.20	$N_2^{2+}: A' \ ^3\Pi_U \rightarrow D \ ^3\Pi_g$	0 - 0	$2\sigma_g^{-1} 1\pi_U^{-1} - 2\sigma_U^{-1} 1\pi_U^{-1}$
55.21	22.46	$N_2^{2+}: A' \ ^3\Pi_U \rightarrow D \ ^3\Pi_g$	1 - 0	$2\sigma_g^{-1} 1\pi_U^{-1} - 2\sigma_U^{-1} 1\pi_U^{-1}$
54.76	22.64	$N_2^{2+}: A' \ ^3\Pi_U \rightarrow D \ ^3\Pi_g$	2 - 0	$2\sigma_g^{-1} 1\pi_U^{-1} - 2\sigma_U^{-1} 1\pi_U^{-1}$
48.56	25.53	$N_2^{2+}: A' \ ^3\Pi_U \rightarrow A \ ^3\Sigma_g^-$	0 - 0	$2\sigma_g^{-1} 1\pi_U^{-1} - ***$

* Using calculations from Ref. (19) and authors' estimates

** Determined from Ref. (17)

*** Lower state not included in Ref. (17)

Qualitatively, the relative strengths of the molecular features can be accounted for by the overlap of the wavefunctions involved in the transitions. Basically, the transition producing the 55.8-nm radiation is



a case which has a very favorable overlap, a fact that can be seen directly by visualization^{26,27} of the wavefunctions of those two orbitals. This situation is

similar to that governing the transition strengths²⁸ associated with KrF* in which the $^2\Sigma \rightarrow ^2\Sigma$ amplitude dominates on account of the extremely good overlap²⁸ existing for these wavefunctions. In contrast, the $X'^2\Sigma_g - A'^2\Pi_u$ transition in N_2^+ corresponds to $2\sigma_g^{-1} \rightarrow 1\pi_u^{-1}$. In this transition, the amplitude is expected to be relatively weak, since the wavefunctions of the initial and final states have a poor overlap²⁷ resulting in a small transition probability. Finally, of the lower states with a $2\sigma_u$ hole (D,E,G $^3\Pi_g$), the D $^3\Pi_g$ state has the best internuclear separation for a favorable Franck-Condon factor, a point that is discussed below. With these considerations, it is clear that the strongest transition in Table II will be the $A'^3\Pi_u \rightarrow D'^3\Pi_g$ at 55.8 nm.

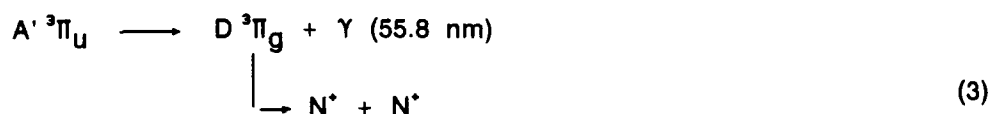
The hypothesis that emerges from this analysis is that the 55.8-nm radiation originates from a quasi-bound level of N_2^{2+} having a $(2\sigma_g^{-1}, 1\pi_u^{-1})$ configuration which undergoes a bound-bound transition terminating on the D $^3\Pi_g$ level associated with the $N^+ + N^+$ asymptote. In addition, the previous studies of ionic fragmentation,⁶ combined with the absence of the transition under comparable experimental conditions with N_2O , indicate that the $2\sigma_g$ vacancy is produced by a direct multiphoton process in N_2 leading to an excited state of $(N^{2+} + N)$ character.

d. Analysis of the Transition

Having specified the states involved in the observed transition, several additional details have been examined, all of which strengthen the identification made above and make possible the construction of the energy level diagram shown in Fig. (3). The width of the 55.8-nm line cannot be due to vibrational structure as the spacing of the lines would be too large.²⁹ On the other hand, a splitting due to rotations would be too small.²⁹⁻³⁰ In fact, the only interaction with the correct energy scale to explain the width of the 55.8-nm line is the spin-orbit interaction.³¹ Since the $A'^3\Pi_u$ state appears to correlate with the $N^{2+} + N$ asymptote,

we can estimate the spin-orbit splitting³² by that of the $N^{2+} \ ^3P_{2,1,0}$ triplet, the value of which is $\sim 175 \text{ cm}^{-1}$. Taking into account the spin-orbit splitting, as well as the resolution of the spectrometer-detector system, the transition would have an observed width of $\sim 0.2 \text{ nm}$. Although this is slightly less than the observed width of the 55.8-nm line, the flat nature of the $D \ ^3\Pi_g$ level may contribute some additional bound-free character to the transition which would increase its width.

The 55.8-nm band arising from the $A' \ ^3\Pi_u \rightarrow D \ ^3\Pi_g$ transition has several properties that are directly analogous to the rare-gas-halogen excimers. The A' state with a charge-transfer ($N^{2+} + N$) nature tends naturally, as a consequence of the polarization attraction, to develop a strong binding character. Conversely, the D level, which correlates to the $N^* + N^*$ asymptote, tends to be repulsive on account of the coulombic force. The difference between these two states is the transfer of one electron between the two atoms. Viewed in analogy with neutral systems, the upper level ($N^{2+} + N$), on account of the charge transfer, represents an ionic bond in comparison to the relatively less bonding forces in the lower ($N^* + N^*$) state. With this line of reasoning, the radiative transition between the two levels



amounts to a transfer of an electron from one atom in the molecule to the other. This results in a dipole transition amplitude μ which is given approximately by the product of the molecular internuclear separation r and the electronic charge e . If, in this case, $r \approx r_0$, the equilibrium value for N_2 , μ would be approximately equal to er_0 , a very large value²⁸ that would naturally lead to efficient emission and, consequently, a bright line in the experimental data. This value of the

dipole amplitude sets a lower bound of ~ 20 psec on the radiative lifetime³³ associated with the 55.8-nm band.

Experimental data taken at high pressure provides an upper bound for the radiative lifetime. The spectrum in Fig. (1), taken at a target gas density of $\sim 1.4 \times 10^{19} \text{ cm}^{-3}$, shows a strong feature at 57.44 nm corresponding to the $\text{N}^* 2p^2 - 2p3d (^1F^o)$ transition.²³ The radiative lifetime³⁴ of the $2p3d (^1F^o)$ state is ~ 285 ps. However, in a spectrum taken at the higher density of $\sim 5.7 \times 10^{19} \text{ cm}^{-3}$, the relative strength of the 57.44-nm N^* line has decreased significantly in comparison to the 55.8-nm N_2^{2+} band. We presume that collisional processes are now sufficiently rapid and can compete with the radiative channel. If we assume that a comparable collisional cross section governs the quenching of the $\text{N}_2^{2+} A' ^3\Pi_u$ level, the change in relative strengths of the molecular and atomic emissions indicates that the radiative lifetime of the $\text{N}_2^{2+} (A')$ level is somewhat less than the $\text{N}^* 2p3d (^1F^o)$ state. With these two bounds, the radiative lifetime of the $\text{N}_2 A' ^3\Pi_u$ level is estimated to be ~ 100 ps.

The shape of the $\text{N}_2 A' ^3\Pi_u$ potential energy curve can be estimated¹⁸ from the $A' ^2\Pi_u$ state in N_2^+ on account of their similar electronic configurations. The only difference between these two configurations is the presence of a $2\sigma_g$ hole in the $A' ^3\Pi_u$. Since the $2\sigma_g$ hole is rather deeply bound, its influence on the molecular bond and, consequently, on the shape of the $A' ^3\Pi_u$ curve, is expected to be small. With this consideration, the vibrational constants of these two levels, at least for low vibrational states, would be approximately equal with a magnitude of $\sim 1900 \text{ cm}^{-1}$, the value³⁵ for the $\text{N}_2^+ A' ^2\Pi_u$ state. Furthermore, the equilibrium internuclear separation of the $\text{N}_2 A' ^3\Pi_u$ state would be close to that of $A' ^2\Pi_u$, which for the latter is $\sim 1.2 \text{ \AA}$. The lower state, $D' ^3\Pi_g$, is also calculated¹⁹ to have an equilibrium separation of $\sim 1.2 \text{ \AA}$ and only one vibrational level. The

nearly equal equilibrium separations of these two levels (A' and D) naturally makes the Franck-Condon factor largest for the $v = 0$ to $v' = 0$ transition with reduced probabilities for the $1 \rightarrow 0$ and $2 \rightarrow 0$ transitions. For this situation, the resulting vibrational spectrum would have a main line at 55.8 nm and perhaps two weaker blue shifted lines at 55.3 nm and 54.7 nm. Precisely this pattern of lines is seen in Fig. (1). This assignment also indicates that the molecular excitation occurs, at least up to an energy of ~ 70 eV, with only a very modest (~ 0.1 Å) expansion of the intermolecular separation, a finding in agreement with the earlier ion studies.⁶

A confirmation of this analysis of the vibrational structure comes from a close examination of the spectrum of N_2O . Although these three lines in the 55-nm region are not seen in N_2O at $1.4 \times 10^{19} \text{ cm}^{-3}$ (the typical density used in these studies), at $5.7 \times 10^{19} \text{ cm}^{-3}$ the lines do appear, implying that there is a small probability, compared to N_2 , of producing excited N_2^{2*} from N_2O . This is not entirely unexpected, since the structure of N_2O is N-N-O and the adiabatic binding energy³⁶ of the oxygen atom is quite weak ($\sim 1.67\text{eV}$). However, the 55.3-nm line is now the strongest, next the 55.8-nm, with the 54.7-nm line the weakest. This alteration in line strength can be attributed to the fact that the equilibrium internuclear separation of the N atoms in N_2O is somewhat greater³⁶ than in N_2 , a condition which would change the Franck-Condon factors, favoring the $1 \rightarrow 0$ transition and decreasing the $0 \rightarrow 0$ transition.

We note that this identification also leads to a fuller understanding of another experiment, namely, the previous work on the multiphoton ionization⁶ of N_2 . The $D^3\Pi_g$ ($v' = 0$) state is predicted¹⁹ to have a lifetime against dissociation into the $N^* + N^*$ channel of $\sim 10^{-13}$ s. Therefore, any $D^3\Pi_g$ produced by radiative decay of the $A'^3\Pi_u$ state will manifest itself as a contribution to the N^* ion spectrum at an energy that is readily derived from knowledge of the $D^3\Pi_g$ minimum

and the corresponding $N^* + N^*$ asymptote. Since the $D^3\Pi_g$ has a potential minimum of ~ 46.4 eV and the $N^* + N^*$ limit is at ~ 38.8 eV, the expected N^* energy is ~ 3.8 eV, one half the difference.

The N^* ion data observed in the previous study⁶ are reproduced in Fig. (4). It is noted that a clearly discernable peak is seen in the 3.7 – 3.8 eV range with a width corresponding closely to the estimated instrumental resolution (~ 0.5 eV). While this peak could be attributed to direct population of the $D^3\Pi_g$ level, it was not seen in photofragment spectroscopy³⁷ of N_2^{2+} . In contrast, N^* fragments in the 3.1 – 3.4 eV range associated with low lying levels of N_2^{2+} were seen in both experiments implying that the 3.8 eV peak does not result from the direct population of the $D^3\Pi_g$ state. These data are, then, consistent with $D^3\Pi_g$ being the lower level of the 55.8-nm transitions. In addition, the integrated strength of the 3.7–3.8 eV ion peak is roughly one percent of the total ion yield, a value in approximate agreement with the fractional yield of the 55.8-nm band observed in the total N_2 fluorescence spectrum.

C. Consideration of the Multiquantum Strong-Field Mode of Excitation

Two important conclusions concerning the character of strong-field multiquantum coupling stem from the discussion given in Section II.B above. They involve (1) the ability to selectively excite inner electrons and (2) the general nature of the strong-field coupling to molecules.

1. Inner-Electron Excitation

The observation of new band radiation at 55.8 nm from transitions involving inner-orbitals in N_2^* and N_2^{2+} , produced by a direct multiphoton process involving N_2 in reactions of the form

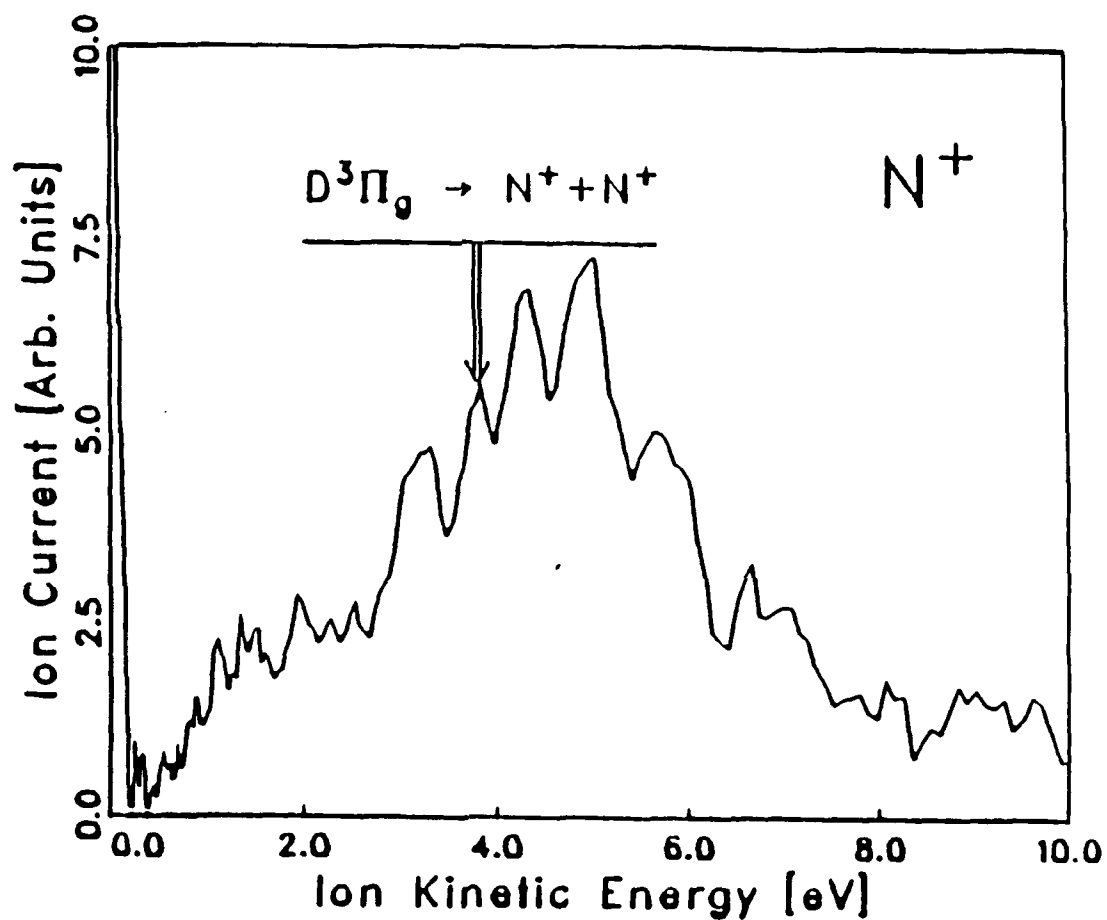
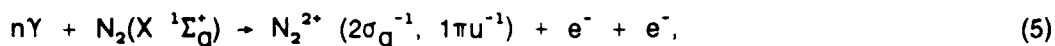


Fig. (4): Kinetic energy distribution of N^+ fragments from Ref. (6) showing the peak at 3.8 eV identified in this proposal. The peak around 3.2 eV is discussed in the text, Ref. (37) and Ref. (19). The structure above 4.0 eV is discussed in Appendix B.



and



provides strong evidence that deeply bound electrons, in this case $2\sigma_g$, can be directly excited^{4,38} by strong-field processes without extensive loss of more weakly bound outer valence electrons. It is expected that this feature of the interaction will manifest itself in many materials and further experiments are being undertaken to test this hypothesis. Conventional pictures of multiphoton processes, particularly those involving the sequential emission of outer electrons from the system, do not provide a basis for understanding these results. Moreover, although N_2 has been one of the most common subjects of spectroscopic analysis for nearly a century, it is striking that the 55.8 nm band was one of the strongest features in the spectrum, but had never previously been observed. These facts suggest the presence of an important new feature in the mechanism of coupling. We now examine that aspect.

2. General Features of Strong-Field Coupling

In addition to providing specific data on N_2 and its ions, the information obtained from the studies of ion production⁶ and fluorescence described above in Section II.B leads to an important general statement concerning the basic character of molecular multiphoton interactions in the strong-field ($\epsilon > e/a_0^2$) regime. Through comparison with electron and ion collisional processes, it will be shown that there is a large class of excitations which can be strongly excited only by strong-field coupling. Therefore, new states of excitation uniquely produced by the strong-field mode of interaction are generally expected for all molecular materials regardless of structure or composition. Furthermore, it will be seen

that the excited states produced naturally by this form of interaction will commonly embody highly asymmetric charge distributions.

The comparison³⁹ with charged-particle collisions can be accomplished in two ways, both of which express different aspects of the dynamics of coupling. One examines the pattern of the electric force developed during the collision while the other represents the encounters graphically in terms of variables describing (1) the maximum electric field ϵ_m produced and (2) the energy transfer E_t communicated to the molecular system during the collisional event.

Consider the ion-molecule (N_2) collisional process illustrated in Fig. (5a) involving an ion having charge Ze and velocity v colliding with impact parameter b . We assume that the ion follows a classical straight-line trajectory approximately perpendicular to the molecular axis. As the collision proceeds, the electric field from the ion experienced by the molecule varies appreciably in both magnitude and direction. Only at point B on the trajectory is the field aligned along the molecular axis. Otherwise the direction of the force on the molecular electrons deviates considerably from the molecular axis. The situation can be made more favorable for the excitation of electronic motions along the molecular axis by going to large impact parameter ($b \gg r_0$), but then the maximum collision field

$$\epsilon_m = \frac{Ze}{b^2} \quad (6)$$

is greatly reduced.

The electric field of a short-duration (τ_p) intense pulse of radiation polarized along the molecular axis represents a qualitatively different type of interaction. In this case, the resulting force field acts primarily to excite electronic motions along the molecular axis. For a sufficiently short pulse, normally in the $\tau_p < 1$ ps range, the effect of molecular rotation for thermally excited levels at normal temperatures

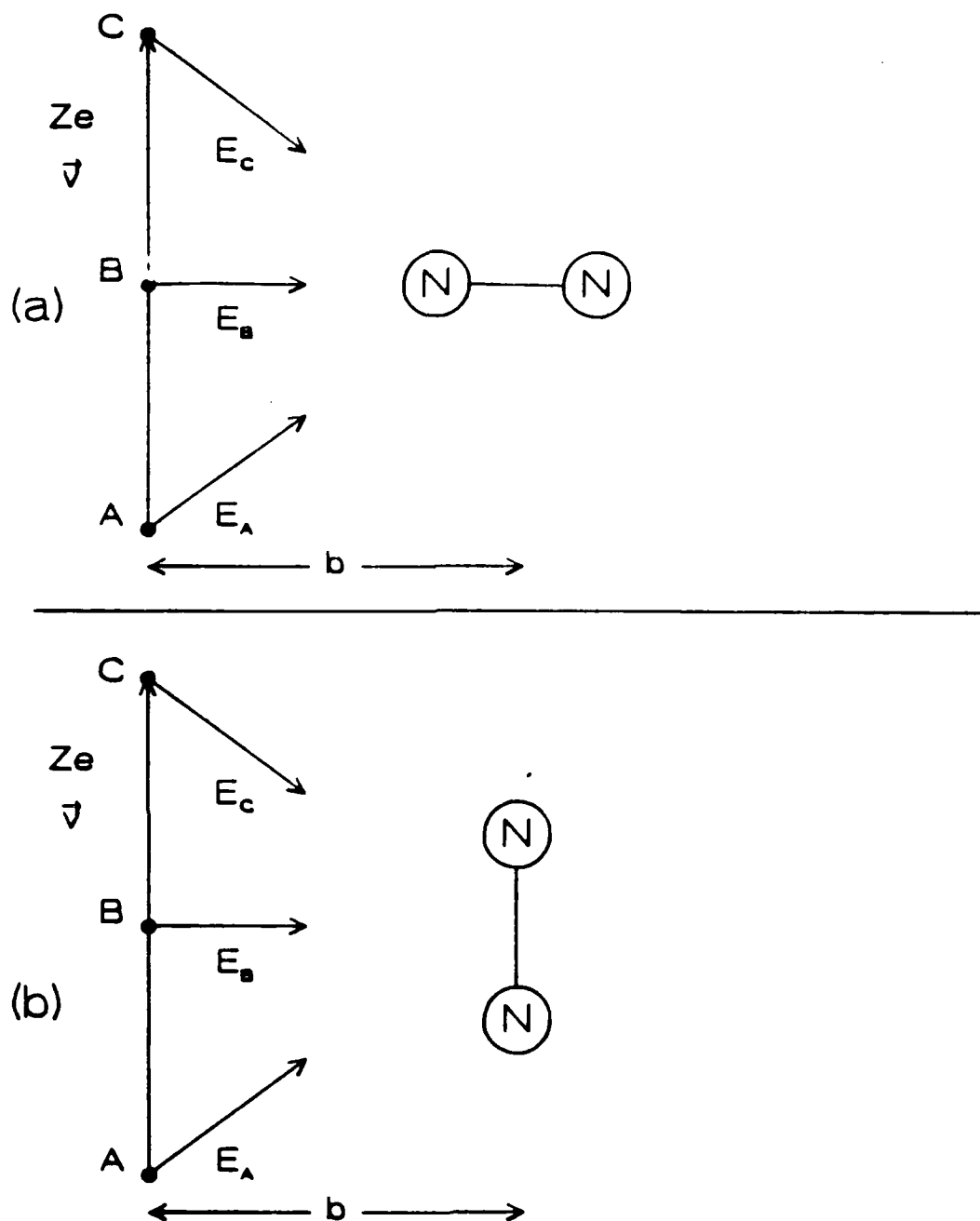


Fig. (5): Geometry of ion-molecule (N_2) collisions showing the changing electric fields experienced by the target during the collision event. (a) Ionic trajectory perpendicular to molecular axis; (b) ionic trajectory parallel to molecular axis.

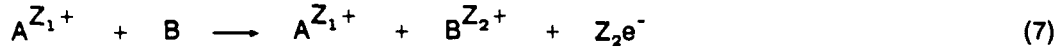
is negligible for almost all molecular materials. This can be seen by noting that molecular rotational frequencies ν_r are given approximately by $\nu_r \approx 2BJ$ for rotational constant B and angular momentum J . With the exception of the hydrides, if we take $B \sim 1 \text{ cm}^{-1}$ as a typical value,³⁵ $\nu_r \tau_p \ll 1$ even for $J = 10$.

Further comparison is shown in Fig. (5b) for the case involving a parallel orientation of the ionic trajectory and the molecular axis. The main effect in this orientation is a force transverse to the molecular axis. Although the field can have an appreciable component along the molecular axis in the limit $b \rightarrow 0$, this situation has a vanishing probability of collision. In addition, as shown below, such close encounters with charged particles, particularly ions, differ from the strong-field coupling in another important way, since they generally impart a substantial recoil energy to the molecular system.⁴⁰ In sharp contrast, the strong-field coupling, although capable of exerting a force with a magnitude representative of ion collisions,³⁹ is extremely ineffective in transferring kinetic energy directly to the target molecule or its constituent atoms.

The differences between the charged-particle collisional processes and the strong-field radiative interaction can be further understood by determining the relationship between kinetic energy transferred to the target system and the strength of the peak electric field occurring in the interaction. To find this relationship, these two processes can be parameterized by the peak field strength, ϵ_m , and the effective duration of the interaction, τ . For a given field strength, we set the interaction times equal for the two processes so that the comparison is made for a fixed transition probability. In the case of the strong-field process, the studies of ion fragmentation⁶ described in Appendix B indicated that the interaction time can be taken as approximately comparable to a period of the

electromagnetic wave $\tau \approx \lambda/c$, while the corresponding field strength is given by $\epsilon_m = (4\pi I/c)^{1/2}$ in which I is the laser intensity.

For the charged particle collisions, we consider a process of the form



in which a projectile ion A of charge Z_1 collides with a neutral system B at rest producing a recoiling ion B^{Z_2+} with the collateral generation of Z_2 electrons. The recoil energy E_t of the target system B , for a projectile with energy E at impact parameter b , is given^{40,41} approximately by

$$E_t \approx \frac{Z_1^2 Z_2^2 e^4 M_A}{E M_B b^2}, \quad (8)$$

with M_A and M_B representing the masses of the particles A and B , respectively, and e denoting the electronic charge. The time-scale of the collisional interaction will be given by

$$\tau = \left(\frac{b^2 M_A}{2E} \right)^{1/2}. \quad (9)$$

The combination of Eqs. (6), (8), and (9) gives the desired relationship between E_t and ϵ_m , namely,

$$E_t = \frac{Z_2^2 e^2}{M_B} \tau^2 \epsilon_m^2. \quad (10)$$

Interestingly, the energy transfer E_t is independent of the nature of the charged projectile. The final connection between the strong-field interaction and the charged-particle collision is obtained by setting the time scale of the collision equal to λ/c which yields

$$E_t = Z_2^2 e^2 \left(\frac{(e^2/a_0)^2}{M_B c^2} \right) \left(\frac{\lambda}{a_0} \right)^2 \quad (11)$$

where f is the maximum field strength in atomic units.

The validity of Eq. (11), for the simple collisional picture used, requires that

$$\frac{\Delta q}{M_A v_A} \ll 1 \quad (12)$$

where Δq is the momentum transfer occurring in the collision and v_A is the velocity of the projectile. Using Eqs. (6), (10), and (11), we find that

$$\frac{\Delta q}{M_A v_A} = \left(\frac{Z_2^2 f^3}{Z_1} \right)^{1/2} \left(\frac{\lambda^2}{a_0^2} \right) \left(\frac{e^2/a_0}{M_A c^2} \right) \quad (13)$$

If we take $Z_2^2/Z_1 \sim 1$ as a characteristic example, Eq. (12) is satisfied for $f \leq 30$. Actually, for field strengths greater than ~ 30 atomic units, the energy transfer will actually be greater than that given by Eq. (11). Thus, Eq. (11) represents a lower bound for charged-particle collisions. Furthermore, since the characteristics of the projectile do not appear in Eq. (11), this relationship is also valid for electron collisions.

We now examine the magnitude of other physical processes which can impart energy transfer to atomic or molecular systems. Generally, for the electron collisions, the emission of Auger electrons will impart a recoil energy exceeding that arising from the incident electron, the magnitude of which can be readily estimated from the kinematics of two-body decay. If we assume that an electron with mass m_e is emitted with an Auger energy E_a , then

$$E_t \approx E_a \left(\frac{m_e}{M_B} \right) \quad (14)$$

In order to estimate an upper bound, we will assume an energy scale for E_a on the order of the K-edge. In this case, for light materials in which the Auger yields arising from a K-vacancy are high, a system such as Ne ($\hbar\omega_K \approx 870$ eV),

gives $E_t \approx 24$ meV, a value almost exactly equal to the mean thermal energy at 300 K.

For heavy materials, such as uranium, since radiative yields dominate the decay of K-shell vacancies, the recoil developed is given approximately by

$$E_t \approx \frac{(\hbar\omega_K)^2}{2Mc^2} \quad (15)$$

where $\hbar\omega_K$ is the emitted photon energy and M is the molecular mass. For U, Eq. (15) gives $E_t \approx 30$ meV, a magnitude close to that arising from Auger decay in light elements. L-shell Auger decay from U (~ 21 keV) gives $E_t \approx 46$ meV, so it is also in the same range. Less energetic excitations arising from electron scattering will, of course, produce smaller recoil energies. Overall, for a wide range of scattering conditions and materials, the recoil energies induced by electron scattering will fall in the range $\sim 3 \times 10^{-5} \leq E_t \leq 5 \times 10^{-2}$ eV.

The recoil energy imparted to an ion during multiphoton ionization is naturally expected to be small, since the incident photons carry very little momentum. For a given number N of quanta absorbed with energy $\hbar\omega$, the recoil is expressed as

$$E_t \approx \frac{(N\hbar\omega)^2}{2Mc^2} \quad (16)$$

the multiquantum counterpart of Eq. (15). From the previous discussion, for a total energy such that $N\hbar\omega = \hbar\omega_K$, E_t is less than 30 meV for all materials.

Two additional mechanisms can communicate recoil energy to the ion produced by multiphoton ionization. They are (1) the interaction of the field-driven ionized electron with the ion, a process equivalent to inverse-bremsstrahlung in the field of the ion, and (2) the subsequent emission of Auger electrons similar to that discussed above in relation to electron collisions. Since the latter can be associated

with essentially the same bounds as the electron scattering case, we now consider the former.

During the inverse-bremsstrahlung process a photon ($\hbar\omega$) is absorbed with the resulting energy appearing in the kinetic energy of the electron-ion pair. Assuming the ion to be structureless, this is a form of elastic electron scattering for which the resulting recoil can be approximately estimated from Eq. (8) provided that it is possible to determine appropriate values for the electron energy E and the impact parameter b . In terms of the particle energy, we can associate the average energy of driven motion with the ponderomotive potential. For radiation at 248 nm, an intensity of 10^{18} W/cm² gives an equivalent ponderomotive potential of 57 eV.

Measurements⁶ of ion energy distributions for N_2^{2+} ions give an upper bound on $E_t \approx 60$ meV and, therefore, a lower limit on the effective value of b . For N_2^{2+} irradiated at 248 nm for ~ 600 ps at an intensity of $\sim 10^{18}$ W/cm², with $Z_1 = 1$, $Z_2 = 2$, $E \approx 57$ eV, and $M_A = m_e$, Eq. (8) gives $b \geq 0.1 a_0$. This value of the impact parameter is expected to be a considerable underestimate, since the experimental bound on E_t was instrumentally limited.⁶ We now scale, for a fixed value of this impact parameter, to fully ionized uranium ($Z_2 = 92$) and let $I \approx 10^{21}$ W/cm² ($\epsilon_m \approx 170$), a procedure which gives $E_t < 1$ meV. Even accounting for multiple electron emission, most of which occurs for rather low values of Z_2 , it is unlikely that the recoil will be above the experimental bound established for N_2^{2+} , namely, within a factor of two of the thermal energy for $T = 300$ K. This places an upper bound on the kinetic energy transfer associated with the strong-field coupling to be on the order of those arising in the case of electron scattering.

We observe that any ion will also experience a ponderomotive potential in the high intensity wave. For a proton irradiated with 248 nm radiation at an

intensity of 10^{21} W/cm², the ponderomotive potential is ~ 3.1 keV. This energy, however, is fully returned^{42,43} to the radiation field during the course of the pulse so that no net displacement of any molecular ions, regardless of charge or mass, will occur as a result of the ponderomotive potential.

This analysis leads to the following general conclusions. Ion collisions can present strong forces ($\epsilon_m \gg 1$) and large recoil energies while electron collisions generate relatively weak forces ($\epsilon_m \leq 1$) and correspondingly small recoil effects. Furthermore, both of these scattering processes are ineffective in exciting organized electronic motions along specific molecular axes. In comparison, since the short-pulse strong field excitation (1) can generate a high force strength ($\epsilon_m \gg 1$), (2) communicates a recoil energy which is very small in relation to molecular bond strengths, and (3) readily excites large scale electronic motions along specific molecular directions, it represents a unique domain of interaction.

These respective regions of interaction can be conveniently displayed in the $\epsilon_m - E_t$ plane shown in Fig. (6). In this picture, the strong-field multiquantum coupling ($\epsilon_m \geq 1$) clearly represents a distinct regime of interaction that is totally unachievable with charged particle collisions and permits strong electronic forces to be applied to a system whose molecular frame can remain intact. It is this situation, in combination with the dynamical features illustrated in Fig. (5), that enables the strong-field coupling to efficiently produce new modes of excitation in molecular materials. The region corresponding to the experiments on N₂, as shown in Fig. (6), clearly falls in this new zone. It is this feature of the interaction which can account for the otherwise anomalous appearance of the $2\sigma_g$ vacancies and the 55.8 nm emission. Although N₂ has served as a specific example, such processes are expected to occur generally for all materials regardless of structure or composition. Given the nature of this form of excitation, it is particularly

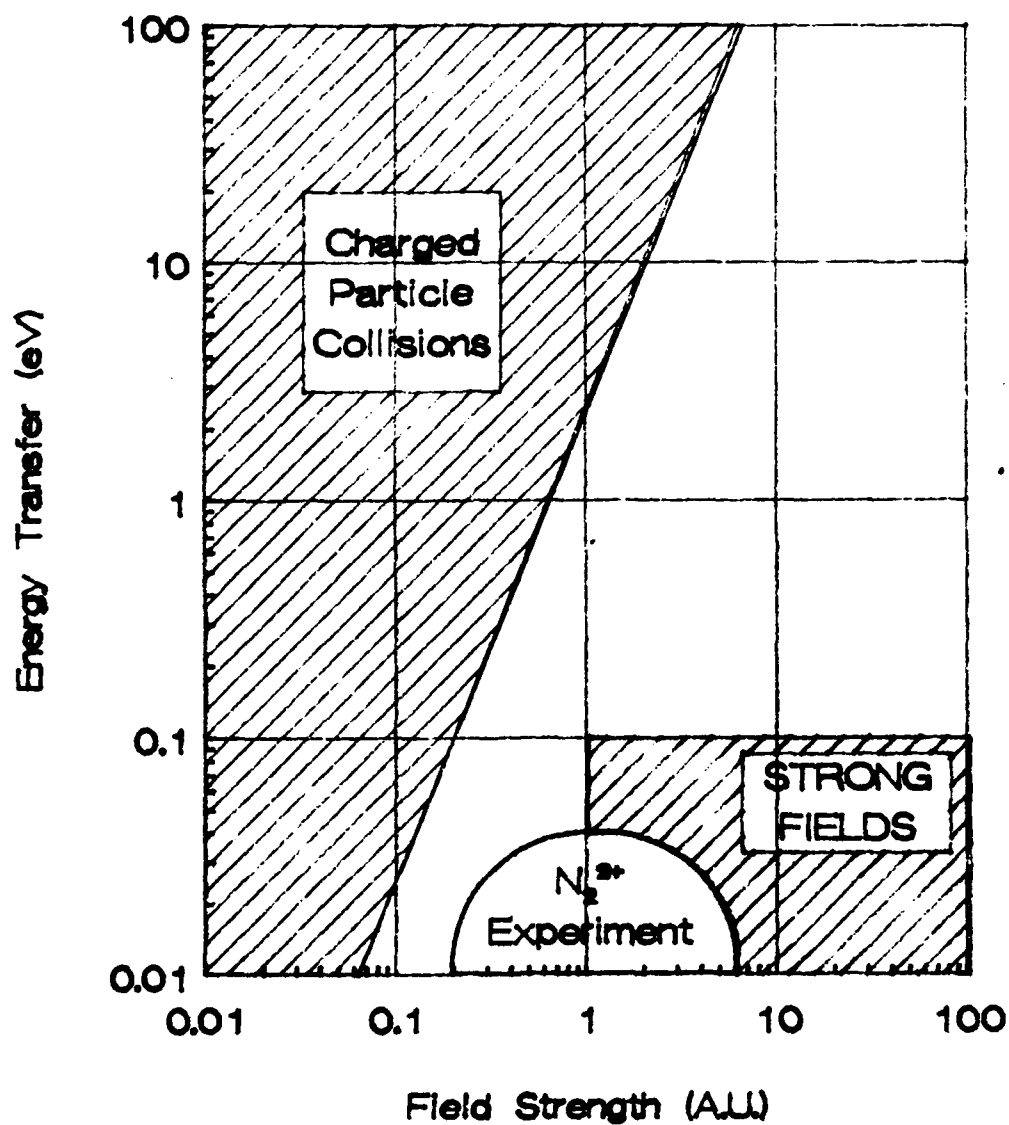


Fig. (6): Display of the comparison of the energy transfer versus electric field strength for charged particle collisions and strong-field interactions, including the influence of Auger events and inverse-bremsstrahlung. Clearly, strong-field interactions lie in a region totally inaccessible by the collisional processes. The region of the N_2 experiments discussed in the text is shown. The parameters for the ion boundary stemming from Eq. (11) correspond to $\lambda = 248$ nm and the other data conforming to the N_2^{2+} case.

well suited for the direct generation of states involving a very large charge asymmetry, such as that represented in N_2 by Eq. (1).

III. CONCLUSIONS

A new ultrahigh intensity subpicosecond laser technology is now available for the study of atomic and molecular interactions in the strong-field regime for which the peak optical field is considerably above an atomic unit (e/a_0^2). It was anticipated that such conditions would produce unusual excited states of matter and that expectation has been confirmed by recent experimental findings revealing the direct multiphoton production of inner-orbital ($2\sigma_g^{-1}$) excited states of N_2^+ and N_2^{2+} . Indeed, it can be shown that the strong-field coupling represents a unique mode of interaction which combines (1) the application of strong electromagnetic forces with (2) a very small collateral transfer of energy. This regime is impossible to achieve with charged particle collisions or with low intensity radiation of any frequency. Interactions of this type are particularly effective in exciting electronic motions along specific molecular axes enabling the generation of new forms of highly excited matter regardless of molecular structure or composition.

IV. REFERENCES

1. T. S. Luk, A. McPherson, G. Gibson, K. Boyer and C. K. Rhodes, "Ultrahigh Intensity KrF* Laser System," submitted to Optics Letters.
2. C. K. Rhodes, "Multiphoton Ionization of Atoms," *Science* **229**, 1345 (1985).
3. C. K. Rhodes, "Ordered Many-Electron Motions in Atoms and X-Ray Lasers," in *Giant Resonances in Atoms, Molecules, and Solids*, ed. J.-P. Connerade, J. M. Esteve, and R. C. Karnatak (Plenum Press, New York, 1987) p. 533.
4. K. Boyer and C. K. Rhodes, "Atomic Inner-Shell Excitation Induced by Coherent Motion of Outer-Shell Electrons," *Phys. Rev. Lett.* **54**, 1490 (1985).
5. C. K. Rhodes, "Physical Processes at High Field Strengths," *Physica Scripta* **T17**, 193 (1987).
6. K. Boyer, T. S. Luk, J. C. Solem, and C. K. Rhodes, "Kinetic Energy Distributions of Ionic Fragments Produced by Subpicosecond Multiphoton Ionization of N_2 ," *Phys. Rev. A* **39**, 1186 (1989).
7. G. Gibson, T. S. Luk, A. McPherson, K. Boyer, and C. K. Rhodes, "Observation of a New Inner-Orbital Molecular Transition at 55.8 nm in N_2^{2+} Produced by Multiphoton Coupling", *Phys. Rev. A*. (In press).
8. M. J. Feldman and R. Y. Chiao, "Single-Cycle Electron Acceleration in Focused Laser Fields," *Phys. Rev.* **A4**, 352 (1971).
9. F. V. Bunkin et A. M. Prokhorov, "Interaction des Electrons avec un Champ Intense de Rayonnement Optique," in *Polarisation, Matière et Rayonnement*, édité par La Societe Française de Physique (Presses Universitaires de France, Paris, 1969) p. 157.
10. E. S. Sarachik and G. T. Schappert, "Classical Theory of Scattering of Intense Laser Radiation by Free-Electrons," *Phys. Rev.* **D1**, 2738 (1970).
11. M. D. Dawson, T. F. Boggess, D. W. Garvey, and A. L. Smirl, "A Hybridly Mode-Locked CW Dye-Laser with Brewster Prisms," *Opt. Commun.* **60**, 79 (1986).
12. K. S. Budil, I. A. McIntyre, and C. K. Rhodes, "Cavity Considerations in Hybridly Mode-Locked Femtosecond Dye Lasers," *Opt. Commun.* **64**, 279 (1987).
13. S. Szatmári, F. P. Schäfer, E. Müller-Horsche and W. Mückenheim, "Hybrid Dye-Excimer Laser System for the Generation of 80 fs, 900 GW Pulses at 248 nm," *Opt. Commun.* **63**, 305 (1987).
14. O. E. Martinez, "3000 Times Grating Compressor with Positive Group Velocity Dispersion: Application to Fiber Compensation in the 1.3 - 1.3 μm Region," *IEEE J. Quantum Electron.* **QE-23**, 59 (1987).

15. O. E. Martinez, "Grating and Prism Compressors in the Case of Finite Beam Size," J. Opt. Soc. Am. B3, 929 (1986).
16. W. Eberhardt, E. W. Plummer, I.-W. Lyo, R. Carr and W. K. Ford, "Auger-Electron-Ion Coincidence Studies of Soft X-Ray-Induced Fragmentation of N₂," Phys. Rev. Lett. 58, 207 (1987).
17. H. Ågren, "On the Interpretation of Molecular Valence Auger Spectra," J. Chem. Phys. 75, 1267 (1981).
18. A. Lofthus and P. H. Krupenie, "The Spectrum of Molecular Nitrogen," J. Phys. Chem. Ref. Data 6, 113 (1977).
19. R. W. Wetmore and R. K. Boyd, "Theoretical Investigation of the Dication of Molecular Nitrogen," J. Phys. Chem, 90, 5540 (1986).
20. C.-M. Liegener, "Calculations on the Auger spectrum of N₂," J. Phys. B 16, 4281 (1983).
21. G. Herzberg, private communication.
22. A. McPherson, G. Gibson, H. Jara, U. Johann, T. S. Luk, I. A. McIntyre, K. Boyer, and C. K. Rhodes, "Studies of Multiphoton Production of Vacuum Ultraviolet Radiation in the Rare Gases," J. Opt. Soc. Am. B 4, 595 (1987).
23. R. L. Kelly, "Atomic and Ionic Spectrum Lines below 2000 Angstroms: Hydrogen through Krypton," Part I, J. Phys. Chem. Ref. Data 16, Suppl. No. 1 (1987).
24. A. McPherson, T. S. Luk, G. Gibson, J. C. Solem, K. Boyer and C. K. Rhodes, "Studies of Strong-Field Effects in Multiphoton Subpicosecond Excited Plasmas: Soft X-Ray Fluorescence and Propagation," in the Proceedings of the Seminar on Fundamentals of Laser Interactions II, edited by F. Ehlotzky, (Springer Verlag, Berlin, in press).
25. K. Siegbahn, C. Nordling, G. Johansson, J. Hedman, P. F. Hedén, K. Hamrin, U. Gelius, T. Bergmark, L. O. Werme, R. Manne and Y. Baer, ESCA Applied to Molecules (North-Holland Publishing Company, London, 1969).
26. R. S. Mulliken and W. C. Ermler, Diatomic Molecules. Results of ab initio Calculations (Academic Press, New York, 1977) p. 127.
27. A. C. Wahl, Science 151, 961 (1966).
28. P. J. Hay and T. H. Dunning, Jr., "The Electronic States of KrF," J. Chem. Phys. 66, 1306 (1977).
29. G. Herzberg, Molecular Spectra and Molecular Structure. I. Spectra of Diatomic Molecules, Second Edition (Van Nostrand, Reinhold Co., New York, 1950).
30. I. Kovacs, Rotational Structure in the Spectra of Diatomic Molecules (Elsevier Publishing Co., New York, 1969).

31. W. G. Richards, H. P. Trivedi and P. L. Cooper, Spin-Orbit Coupling in Molecules (Oxford University Press, London, 1981).
32. C. E. Moore, Atomic Energy Levels, NSRDS-NBS 35 Volume 1, (USGPO, Washington, D. C., 1971).
33. R. D. Cowen, The Theory of Atomic Structure and Spectra (University of California Press, Berkeley, 1981) p. 403.
34. W. L. Wiese, M. W. Smith, and B. M. Glennon, Atomic Transition Probabilities, Volume I, Hydrogen through Neon, NSRDS-NBS 4 (USGPO, Washington, D. C., 1966) p. 59.
35. K. P. Huber and G. Herzberg, Molecular Spectra and Molecular Structure, IV. Constants of Diatomic Molecules (Van Nostrand Reinhold Company, New York, 1979).
36. G. Herzberg, Molecular Spectra and Molecular Structure III. Electronic Spectra and Electronic Structure of Polyatomic Molecules (Van Nostrand Co., New York, 1966) p. 596.
37. P. C. Cosby, R. Möller and H. Helm, "Photofragment Spectroscopy of N_2^{2+} ," *Phys. Rev. A* **28**, 766 (1983).
38. A. Szöke and C. K. Rhodes, "Theoretical Model of Inner-Shell Excitation by Outer-Shell Electrons," *Phys. Rev. Lett.* **56**, 720 (1986).
39. K. Boyer, G. Gibson, H. Jara, T. S. Luk, I. A. McIntyre, A. McPherson, R. Rosman, J. C. Solem, C. K. Rhodes, "Corresponding Aspects of Strong-Field Multiquantum Processes and Ion-Atom Collisions," *IEEE Trans. Plasma Science* **16**, 541 (1988).
40. K.-H. Scharfner, "Highly Charged Recoil Ions," in Fundamental Processes in Energetic Atomic Collisions, edited by H. O. Lutz, J. S. Briggs, and H. Kleinpoppen, Series B, Vol. 103 (Plenum Press, New York, 1983) p. 637.
41. A. S. Schlachter, W. Groh, A. Müller, H. F. Beyer, R. Mann, and R. E. Olson, "Production of Highly Charged Rare-Gas Recoil Ions by 1.4 MeV/amu U^{92+} ," *Phys. Rev. A* **26**, 1373 (1982).
42. T.W.B. Kibble, "Refraction of Electron Beams by Intense Electromagnetic Waves," *Phys. Rev. Lett.* **16**, 1054 (1966).
43. A. Szöke, "Interpretation of Electron Spectra Obtained from Multiphoton Ionization of Atoms in Strong Fields," *J. Phys. B* **18**, L427 (1985).

Appendix A

ULTRAHIGH INTENSITY KrF* LASER SYSTEM*

T. S. Luk, A. McPherson, G. Gibson,
K. Boyer and C. K. Rhodes

Laboratory for Atomic, Molecular, and Radiation Physics
Department of Physics, University of Illinois at Chicago
P. O. Box 4348, Chicago, Illinois 60680

ABSTRACT

The operational characteristics of an ultrahigh intensity subpicosecond large aperture KrF* laser system are described. Measurements show the achievement of a focal spot diameter less than 1.7 μm . Combined with measurements of the pulse width and pulse energy, this yields an average intensity of $\sim 2 \times 10^{19} \text{ W/cm}^2$, a value corresponding to a peak electric field of $\sim 24 (e/a_0)$. Light sources of this nature will find application in a broad range of studies of the nonlinear properties of matter in the strong-field regime.

* to be published in Optics Letters

Rare-gas-halogen systems are well suited for the production of extremely high peak-brightness outputs because they combine efficient energy storage, a broad gain-bandwidth, and a high threshold for the onset of nonlinear processes affecting both losses and the mode of propagation. Although several demonstrations that the confluence of these properties readily results in high peak power have been reported,¹⁻⁷ the generation of high peak intensity requires, in addition, careful control of the spatial character of the output energy. In this Letter, we report the measured focusability of a large aperture subpicosecond KrF* system capable of generating a peak power in excess of 400 GW. With the capability to achieve an average focal intensity of $\sim 2 \times 10^{19}$ W/cm², which corresponds to a peak electric field of $\sim 24 (e/a_0) = 1.2 \times 10^{11}$ V/cm, this system can be used in new areas of study corresponding to a regime for which the applied field significantly exceeds that characteristic of the outer electronic shells in all materials.

The laser system, based on one previously described,² is shown schematically in Fig. (1). The 248-nm seed pulse is generated from a primary source operating at 745 nm by doubling and mixing in the sequence 745 nm \rightarrow 372 nm \rightarrow 248 nm. The 745-nm source is a hybrid mode-locked dye laser with intracavity dispersion compensation⁸ pumped by a cw mode-locked frequency doubled Nd:YAG laser. The dye laser is tuned by intracavity spectral windowing⁹ and generates bandwidth-limited 200 fs pulses. Single 745-nm pulses are amplified in a two-stage dye amplifier which is transversely pumped by a ~ 300 mJ/pulse, frequency doubled, Q-switched Nd:YAG system at a repetition rate of 2 Hz. This amplification produces single pulse energies in the 100 – 150 μ J range. These pulses are focused to a diameter of approximately 1 mm in two KDP crystals, of 1 and 3 mm length, suitably cut² for frequency doubling to 372 nm and sum-frequency mixing to 248 nm, producing 248-nm pulses with an energy of 1 – 2 μ J.

A KrF* excimer preamplifier (Lambda Physik 201 MSC EMG) for the 248-nm pulses is operated with a gas mix of F₂, Kr, and Ne at a pressure of 1500 mbar and with a discharge voltage of 14 kV, producing a gain of ~ 500. This unusual operating pressure and voltage give sufficient amplification while, at the same time, minimizing beam distortion caused by the discharge, a critical factor in the resulting focusability of the laser system. The output from the preamplifier is spatially filtered in vacuum in a diffraction limited manner using a 100- μ m diameter pinhole. This spatial filter, with a transmission of ~ 30 - 40%, furnishes a seed pulse having an energy of 150 - 200 μ J. After the spatial filter the 248-nm pulse is collimated and expanded to a 10 cm diameter using a 10-power reflecting telescope of the Dall-Kirkham design. The final seed pulse, which has a signal/ASE ratio of ~ 4,000:1, is injected into a large aperture KrF* amplifier, a device which has been christened Prometheus. Prometheus was specifically designed to work at relatively low pressure and low gain in order to reduce wavefront distortion and ASE, conditions which are necessary even for the preamplifier as noted above.

Prometheus has two parallel 2.5 m long discharge channels separated by an x-ray gun preionizer. The gas flow between the discharge electrodes is laminar and transverse with a flow rate sufficient to clear the discharge volume ~ 5 times between laser pulses. The laser medium and the electrical insulating oil used in the high voltage enclosure are temperature controlled to minimize thermal gradients and consequent wavefront distortion in the optical path. Although the system has the capability to excite a discharge with a total cross-sectional area of 10 cm x 10 cm, the present device, due to excessive curvature of the electrodes, produces a saturated output only over approximately one third of that area. A measurement of beam distortion at 632 nm with full gas flow, but without the discharge operating, demonstrated an RMS wavefront distortion¹⁰ of $\lambda/13$ over the full aperture. In

addition, no streamers were present in the discharge and an estimate of the nonlinear wavefront distortion occurring at the final output window of the amplifier for $n_2 \approx 10^{-13}$ esu at an intensity of 10 GW/cm^2 gives $\sim \lambda/10$. Further estimates show that the contribution to nonlinear distortion from the amplifier medium, mainly helium, is negligible. Under these conditions, the spatial character of the output beam is governed by that of the seed-beam.

Typical operating conditions employ an x-ray gun voltage of $\sim 115 \text{ kV}$, a discharge voltage of $\sim 180 \text{ kV}$, a pulse repetition rate of 0.4 Hz and a 1.6 atm gas mix of $0.15\% \text{ F}_2/5\% \text{ Kr}/94.85\% \text{ He}$. Measurements give a small signal gain of $\sim 2.9 \text{ \% cm}^{-1}$ and a nonsaturable loss parameter of $0.28\% \text{ cm}^{-1}$. An output energy of $\sim 250 \text{ mJ}$ is produced with an input pulse of $\sim 200 \text{ }\mu\text{J}$. A maximum recorded output of 350 mJ has been observed. The associated ASE, which mainly originates from the power amplifier itself, is small and poorly focusable. The ASE comprises $\sim 10\%$ of the short pulse energy and has a measured minimum focal diameter of $\sim 3 \text{ mm}$.

The duration of the amplified pulse was measured, using two photon fluorescence in high pressure xenon,¹¹ to be 600 fs . The autocorrelation trace is similar to that shown in Ref. (11). Lengthening of the original 200 fsec 745-nm seed pulse is due, at least in part, to group velocity mismatch occurring in the frequency conversion crystals, which are designed for 350 fsec pulses, and the optical components comprising the remainder of the beam path. Efforts are underway to produce shorter pulses by reduction of the crystal length and suitable phase control (chirping) of the seed-beam pulse.

Measurements of the focusability of the seed pulse after passing through Prometheus were made by using a technique similar to that reported by Roberts et al.¹² A central 29-mm portion of the expanded seed-beam was selected and directed

onto a 60-mm focal length aspheric mirror. The amount of energy collected is estimated to be $\gtrsim 100$ nJ and there is no indication of optical breakdown affecting the measurement. The focus of this f/2.07 optical system is imaged by a 15-power reflecting microscope objective (Ealing 25-0506) onto either a CCD camera or a linear photodiode array (Reticon 512G), the latter having a 25 μm square pixel size.

The beam profile at the image plane of the microscope objective is shown in Fig. (2). An understanding of two important instrumental features is needed in order to interpret this measurement. They are (1) the magnitude of the cross-channel coupling due to the tapered aperture response function of the array, a quantity measured with a 5 μm diameter spot from a HeNe laser and found to be 25%, and (2) the asymmetric profile of the photodiode array output due to a transient electronic response characteristic of the pulsed mode. Although a detailed understanding of this transient electronic response is not in hand, a genuinely asymmetric beam profile would reverse direction upon rotation of the diode array 180° about the beam direction. Experimentally no change in the profile results from this operation, verifying that the observed profile asymmetry is an instrumental electronic effect. Furthermore, the focal spot viewed with the CCD camera clearly indicates a uniform circular spot. With these considerations, the spot size of the focus of the 248-nm seed pulse, using the aspheric mirror, is $\gtrsim 1.7$ μm in diameter at 15% of the maximum amplitude.

The combination of the measured 600 fsec pulse length, the 1.7 μm diameter focal spot size, and a value for the laser energy of 250 mJ, gives an average intensity of 2×10^{19} W/cm², a value nearly one thousand times higher than that used in our previous studies.¹³ The ponderomotive potential experienced by a

free electron in 248-nm radiation at this intensity is ~ 114 keV, a value corresponding approximately to the uranium K-edge (115.6 keV).

Measurements of the collision-free multiphoton ionization of Ne clearly demonstrate that a considerable increase in intensity is achieved with the Prometheus system. We recall that when a maximum intensity of $\sim 10^{16}$ W/cm² was available, the highest neon charge state observed¹⁴ was Ne²²⁺. In sharp contrast, Fig. (3) clearly shows the presence of a strong Ne⁸⁺ signal, in this case arising from a single laser shot and for conditions representing less than optimum laser performance. The total energy¹⁵ required to produce Ne⁸⁺ from the neutral atom is ~ 1 keV. The estimated intensity corresponding to this measurement has a value of only $\sim 1 \times 10^{10}$ W/cm², which arises from the use of larger f-number optics and a reduction of pulse energy stemming from geometrical obstruction of the beam in the apparatus used for the ion measurements.

A final observation concerning propagation is pertinent to the focusability of the full amplified output beam. Preliminary studies of the propagation of the 248-nm beam at full power through air have shown that distinct aberrations occur after a distance of $\sim 3 - 4$ m. This distortion is manifested by the appearance of clusters of filaments or hot spots, with diameters in the range of $50 - 100$ μ m, and are easily seen when polaroid film (type 107) is irradiated. Moreover, these filaments form reproducible stable patterns and appear to exist for lengths on the order of many tens of centimeters, or perhaps longer, as evidenced by moving the polaroid film along the beam path. It was possible to eliminate the filamentation completely by passing the beam through a helium atmosphere. Presently, the full power beam is transported to the experimental stations by using beam lines evacuated to a pressure below 1 Torr.

In summary, the operational properties of a high intensity subpicosecond large aperture KrF* system have been experimentally established. Measurements show that for a total output power of ~ 400 GW, a focal intensity exceeding 10^{19} W/cm² can be produced. Refinements of the instrumentation clearly will enable the development of peak intensities considerably in excess of 10^{20} W/cm². Instruments of this nature will certainly find broad application in the study of new strong-field phenomena in atoms, molecules, and plasmas.

The authors gratefully acknowledge I. A. McIntyre's assistance in measurements of the spatial propagation as well as the technical support of P. Noel and J. Wright. Additionally, the authors wish to acknowledge the important efforts of W. Cramer, T. Tiffin, M. Klawitter, G. Murphy, J. Engert, J. Schreckeis, and A. Geier. The Prometheus amplifier was obtained through support from the Division of Advanced Energy Projects, DOE and by the SDIO Office of Directed Energy. Assistance in the procurement of the amplifier from Beta Development Corporation by C. Fenstermacher at the Los Alamos National Laboratory is enthusiastically acknowledged. Other support originated from the AFOSR, the ONR, and the SDIO/IST.

REFERENCES

1. J. G. Glownia, G. Arjavalingham, P. P. Sorokin and J. E. Rothenberg, Opt. Lett. 11, 79 (1986).
2. A. P. Schwarzenbach, T. S. Luk, I. A. McIntyre, U. Johann, A. McPherson, K. Boyer and C. K. Rhodes, Opt. Lett. 11 499 (1986).
3. J. G. Glownia, J. Misevich and P. P. Sorokin, J. Opt. Soc. Am. B4, 1061 (1987).
4. S. Szatmári, F. P. Schäfer, E. Müller-Horsche and W. Muckenheim, Opt. Commun. 63, 305 (1987).
5. J. R. M. Barr, N. J. Everall, C. J. Hooker, I. N. Ross, M. J. Shaw and W. T. Toner, Opt. Commun. 66, 127 (1988).
6. S. Watanabe, A. Endoh, M. Watanabe and N. Sarukara, Opt. Lett. 13, 580 (1988).
7. A. Endoh, M. Watanabe and S. Watanabe, Opt. Lett. 12, 906 (1987).
8. I. A. McIntyre, K. Boyer and C. K. Rhodes, Opt. Commun. 67, 225 (1988).
9. M. D. Dawson, T. F. Boggess, D. W. Garvey and A. L. Smirl, Opt. Lett. 11, 721 (1986).
10. W. Long, Northrop, Inc., private communication.
11. M. H. R. Hutchinson, I. A. McIntyre, G. N. Gibson and C. K. Rhodes, Opt. Lett. 12, 102 (1987).
12. J. P. Roberts, A. J. Taylor, P. H. Y. Lee and R. B. Gibson, Opt. Lett. 13, 734 (1988).
13. A. McPherson, G. Gibson, H. Jara, U. Johann, T. S. Luk, I. A. McIntyre, K. Boyer and C. K. Rhodes, J. Opt. Soc. Am. B4, 595 (1987); K. Boyer, T. S. Luk, J. C. Solem and C. K. Rhodes, Phys. Rev. A39, 1186 (1989).
14. T. S. Luk, M. H. R. Hutchinson, H. Jara, U. Johann, I. A. McIntyre, A. McPherson, A. P. Schwarzenbach, K. Boyer, and C. K. Rhodes, SPIE Vol. 710

Excimer Lasers and Optics (1986), p. 99; C. K. Rhodes, Phys. Scripta T17, 193 (1987).

15. T. A. Carlson, C. W. Nestor, Jr., N. Wasserman and J. D. McDowell, At. Data 2, 63 (1970).

FIGURE CAPTIONS

- Fig. (1): A schematic showing the layout of the ultrahigh intensity KrF* laser system. The diagnostic measurements were performed at the position indicated after the Prometheus amplifier.
- Fig. (2): A 10 shot average of the output of the photodiode array. One pixel represents $1.7 \mu\text{m}$. Interpretation of the signal is described in the text.
- Fig. (3): Charge state spectrum of Ne collected with a time-of-flight spectrometer—showing the Ne^{8+} component using a laser intensity estimated to be $\sim 10^{18} \text{ W/cm}^2$. Satellite signals corresponding to ^{22}Ne ions are also visible. Since ^{22}Ne abundance is less than ten percent, statistical fluctuations occurring for data taken on a single shot cause the ^{22}Ne 7+ and 8+ signals to be absent.

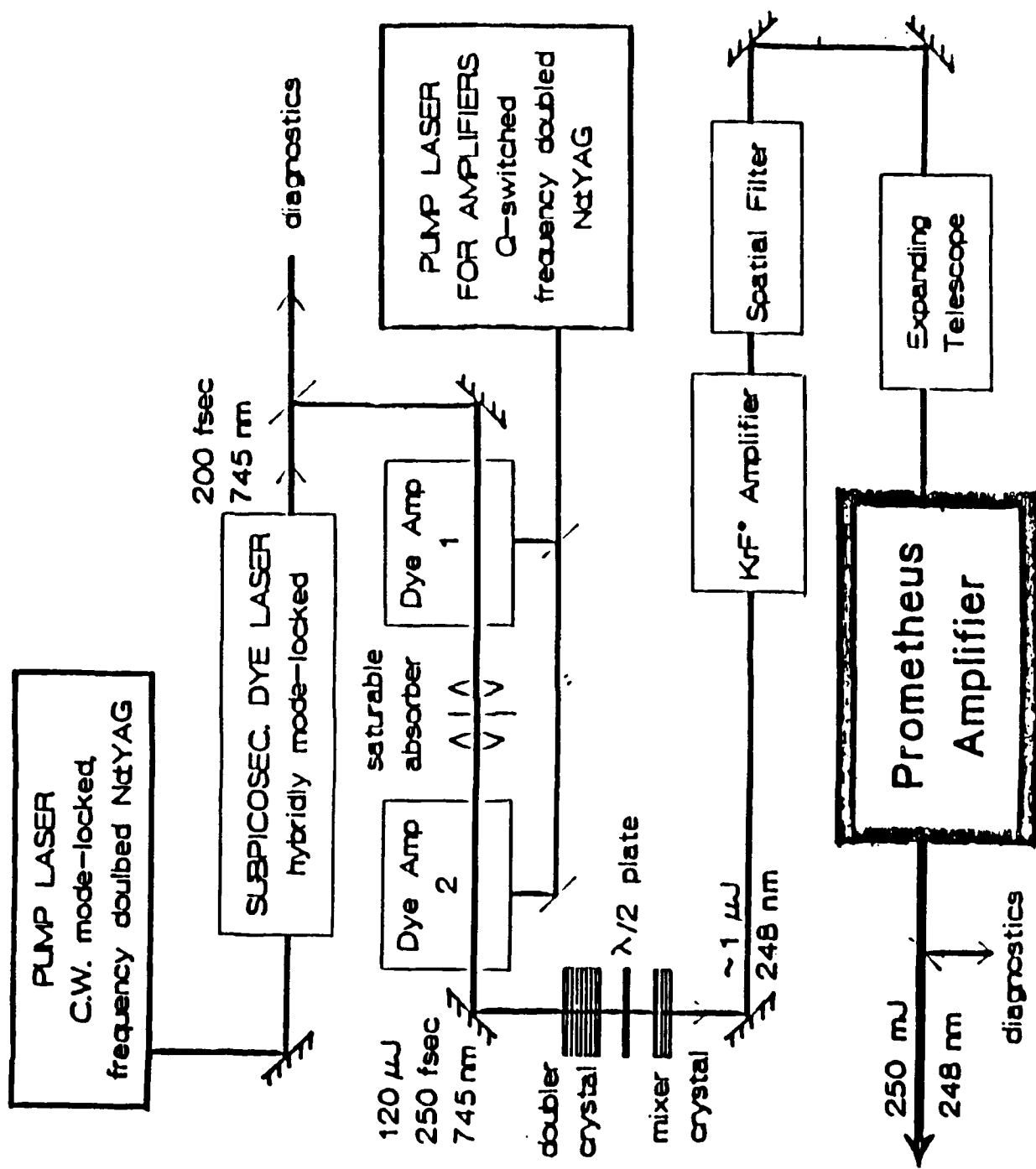
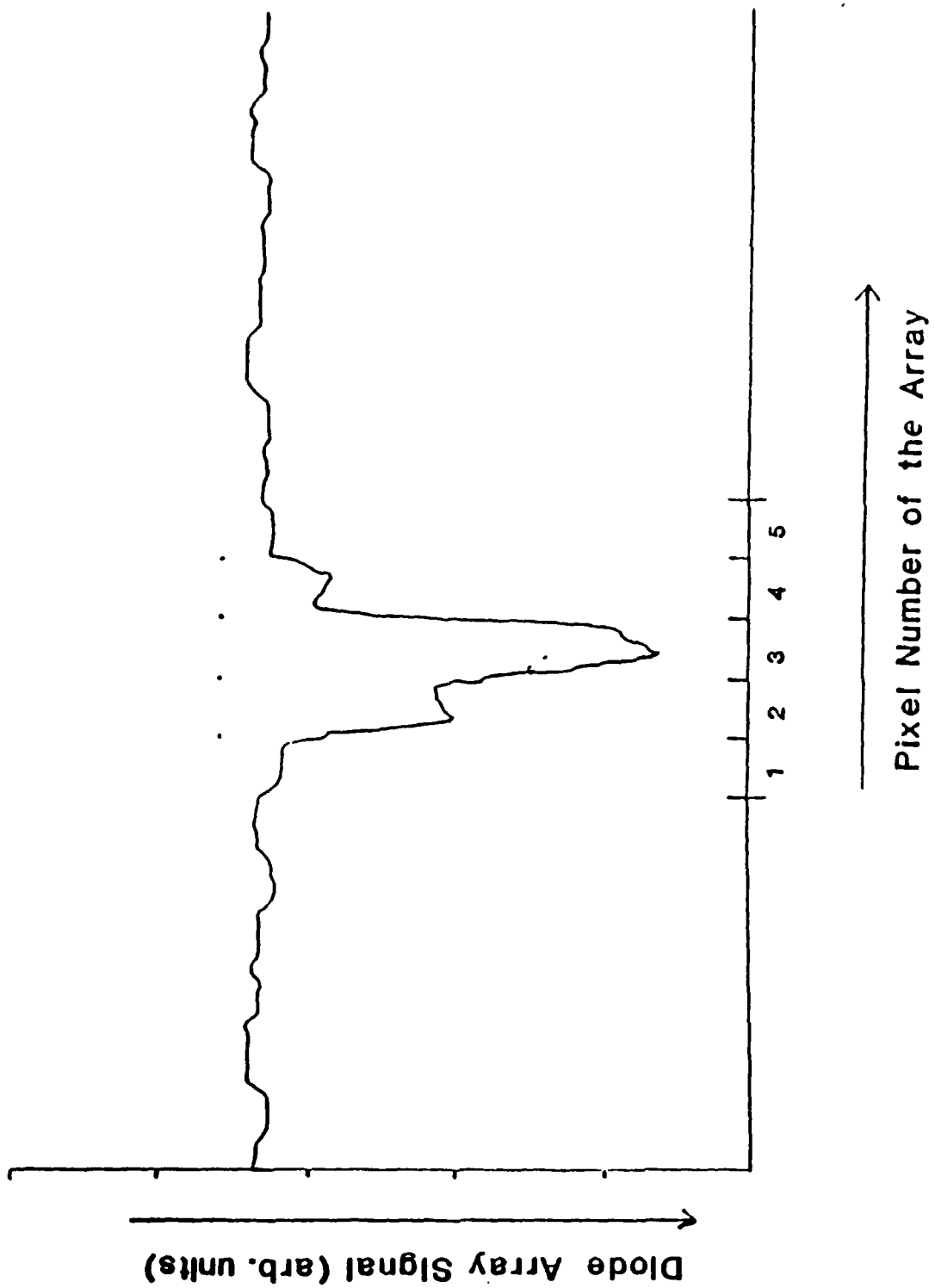
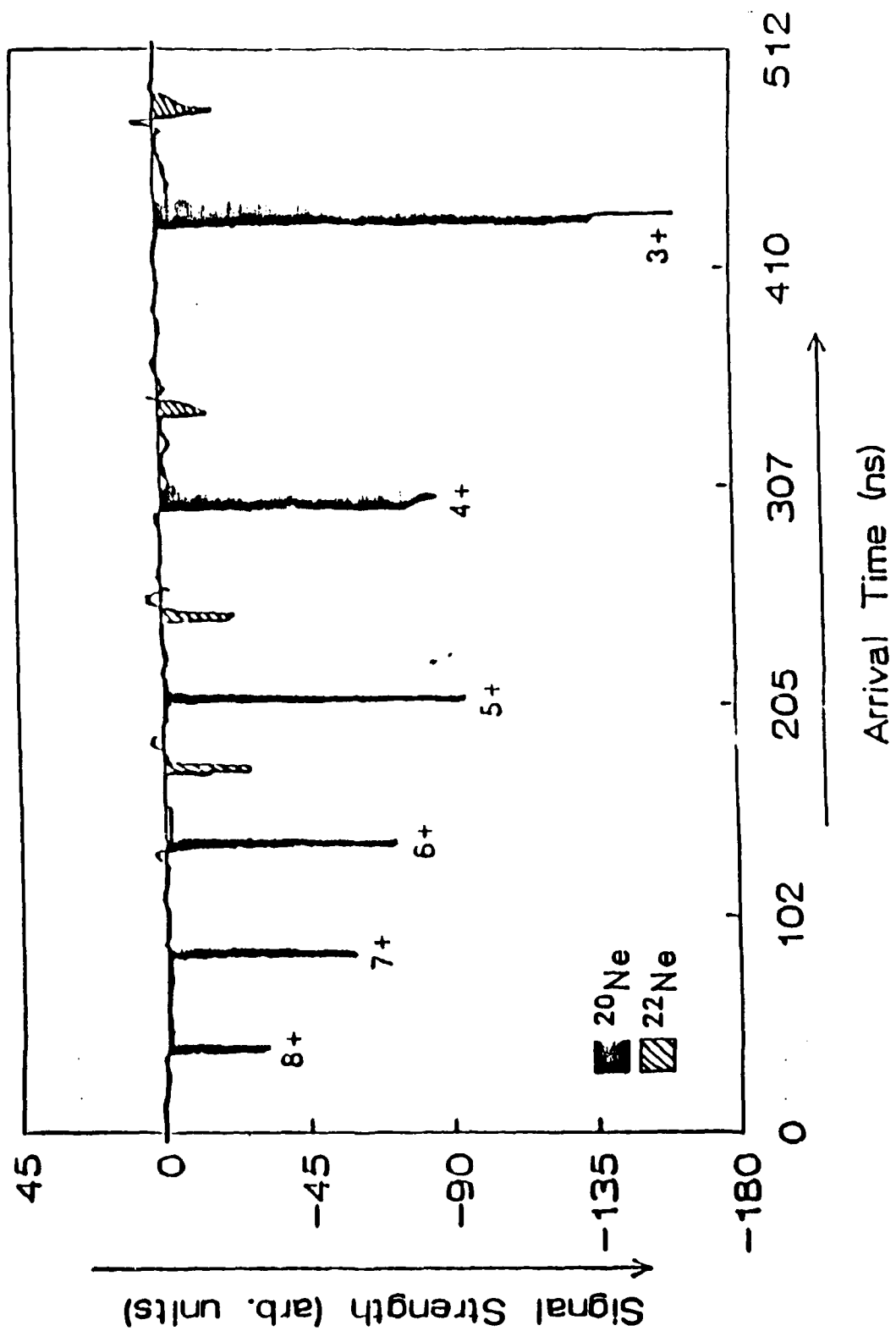


FIGURE 1





Kinetic energy distributions of ionic fragments produced by subpicosecond multiphoton ionization of N_2

K. Boyer, T. S. Luk, J. C. Solem,* and C. K. Rhodes

Laboratory for Atomic, Molecular, and Radiation Physics, Department of Physics, University of Illinois at Chicago, P.O. Box 4348, Chicago, Illinois 60680

(Received 11 July 1988)

A study of the kinetic energy distributions of ionic fragments produced by subpicosecond irradiation of N_2 with 248-nm radiation at an intensity of $\sim 10^{16}$ W/cm² is reported. These measurements, in comparison to other findings involving molecular excitation with charged particles and soft x rays, reveal several important features of the nonlinear coupling. Four ionic dissociative channels are identified from the data on the multiphoton process. They are $N_2^{1+} \rightarrow N^+ + N^+$, $N_2^{2+} \rightarrow N + N^{2+}$, $N_2^{1+} \rightarrow N^+ + N^{2+}$, and $N_2^{4+} \rightarrow N^+ + N^{3+}$, three of which are charge asymmetric. The data for the energy distributions are found to be in approximate conformance with a simple picture involving ionizing transitions occurring within a time of a few cycles of the ultraviolet wave at an internuclear separation close to that of the ground-state ($X^1\Sigma_g^+$) molecule. The implication follows that a strong nonlinear mode of coupling is present which causes a high rate of energy transfer. A simple hypothesis is presented which unites the ability for rapid energy transfer with the observed tendency to produce charge-asymmetric dissociation.

I. INTRODUCTION

Processes involving the rapid production of molecular vacancies generally result in energetic fragmentation of the molecular ion produced. In particular, studies have been made of the fragmentation of N_2 , having the ground-state configuration

$$(1\sigma_g)^2(1\sigma_u)^2(2\sigma_g)^2(2\sigma_u)^2(1\pi_u)^4(3\sigma_g)^2,$$

arising from photon-induced inner-shell excitation,¹⁻³ electron collisions,⁴ and ion collisions.⁵ Rapid molecular ionization by multiphoton processes is also expected to produce ionic fragments with a characteristic distribution of kinetic energies.⁶⁻⁸ Comparison of the energy spectra of the fragments produced by these different means can give information on the corresponding mechanisms of vacancy formation and the dynamics of molecular dissociation. The present study discusses the observation of N^+ , N^{2+} , and N^{3+} fragments produced by multiphoton ionization of N_2 with subpicosecond 248-nm radiation at an intensity of $\sim 10^{16}$ W/cm². These data reveal specific information on the dynamics of these nonlinear molecular events.

Assuming that the molecular potential is dominated by the Coulomb term, the time τ for two atoms, with a reduced mass of M initially situated at a bond distance of $\sim 2\beta a_0$ and ionized suddenly by a pulse of radiation to charge states Z_1 and Z_2 , to undergo a Coulomb explosion^{1,9,10} and develop a separation of x , is

$$\tau \approx \frac{\lambda_c}{c\alpha^2} \left[\frac{\beta^3 M}{2m_e Z_1 Z_2} \right]^{1/2} \times \left[\frac{x(1-2\beta a_0/x)^{1/2}}{2\beta a_0} + \frac{1}{2} \ln \left| \frac{1+(1-2\beta a_0/x)^{1/2}}{1-(1-2\beta a_0/x)^{1/2}} \right| \right]. \quad (1)$$

In Eq. (1), α is the fine-structure constant, m_e the electron mass, λ_c the electron Compton wavelength, a_0 the Bohr radius, and c the speed of light. For $x=1.0$ nm, with $M=7$ amu, $\beta=1$, $Z_1=2$, and $Z_2=1$, Eq. (1) gives $\tau \approx 14.6$ fs. For these parameters, the explosion of a homonuclear diatomic molecule would yield an ion kinetic energy of $U_0=13.6$ eV for each fragment, a magnitude that can be readily measured. In particular, this suggests that information on electron-ionization rates in the femtosecond range associated with the production of the multiply charged ions can be obtained from the kinetic energy distributions of the ionic spectra.⁶⁻⁸

II. EXPERIMENTAL CONSIDERATIONS

In these studies of ion spectra, a subpicosecond 248-nm source¹¹ was used to produce the ionization in a small focal volume under collision-free conditions and the energies of the ions were measured in a time-of-flight spectrometer.¹² In the apparatus for ion detection,¹³ the particles were extracted through a 0.5-mm aperture by a static field of 100 V/cm. An additional potential of 1.3

kV was applied to the ions before entering the 1-m-long free-drift region.

Several factors can contribute to the observed energy resolution of the ion signals.¹⁴ In order to isolate the effect arising from molecular dissociation, the experiments were performed in a regime for which (1) the density was sufficiently low so that the space-charge energy was small and (2) the ion energy was sufficiently high so that the expansion of the ion packet during its flight to the detector was negligible.¹⁴ The proper conditions were established by a study of the resolution obtained for atomic Ar, a species for which the contribution from dissociation is absent. Although the resolution limit arising from the space-charge effect deduced from the N_2^+ data was approximately 0.13 eV for our experimental conditions, the actual value was somewhat greater, since the main source of energy spreading for the energetic ions was due to the time dispersion characteristic of this technique. For 6-eV N^+ ions in our apparatus, the time dispersion is calculated to be 9.6 ns/eV. This figure, together with the electronic width of 5 ns, gives an energy resolution of ~ 0.5 eV. Similarly, resolutions of 1.4 and 3.0 eV are obtained for 10-eV N^{2+} and 20-eV N^{3+} ions, respectively. Furthermore, the absolute energy scale is governed by the ability to determine accurately the arrival time corresponding to zero-initial-energy ions. These considerations result in experimental ion energy resolutions of ~ 1 eV for 6-eV N^+ , ~ 2.8 eV for 10-eV N^{2+} , and ~ 6 eV for 20-eV N^{3+} .

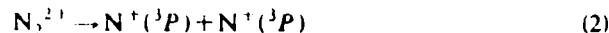
III. EXPERIMENTAL FINDINGS AND DISCUSSION

The time-of-flight data for the N^+ -ion signal are illustrated in Fig. 1(a). Two peaks displaced symmetrically about a central component are clearly observed. Analysis of this signal shows that the prominent central feature comes from ions with a very low kinetic energy and that the two symmetrically placed components correspond to the energetic fragments generated by the molecular dissociation. This is readily seen from comparison of the data in Fig. 1(a) with that shown in Fig. 1(b) for N_2^+ , an ion which should exhibit only a central thermal energy peak, perhaps involving some additional broadening arising from the effect of space charge. The two symmetrically located components of dissociative origin exhibited in Fig. 1(a) result from two velocity groups of ions, one initially headed toward the detector and a corresponding oppositely directed component whose momentum is reversed by the action of the extracting field.^{2,15} Analyses of these peaks for N^+ , N^{2+} , and N^{3+} have been used to determine both (a) the relative abundances and (b) the distributions of kinetic energies arising from the molecular fragmentation.

Integrated over all energies, the relative abundances in percent are 54, 32, and 14 for N^+ , N^{2+} , and N^{3+} , respectively. Interestingly, the ratio $[N^+]/[N^{2+}] \approx 1.7$, a value not far from the minimum magnitude seen (~ 1.9) in the soft-x-ray studies¹ slightly above the nitrogen *K* edge ($\hbar\omega = 440$ eV), but rather far from that observed (~ 4.7) well beyond the *K* edge ($\hbar\omega = 930$ eV) in other work.⁹ A considerably higher fraction of N^{2+} appears to

be produced by the multiphoton mechanism for the conditions of these experiments.

The distributions of the kinetic energies for multiphoton-produced N^+ and N^{2+} ions can be compared to the corresponding distributions observed in the soft-x-ray studies.¹⁻³ Figure 2 illustrates this comparison for N^+ ions which, for the x-ray work, arise from the



channel. All three distributions shown in Fig. 2 have their maximum strengths in the ~ 3.9 – 5.0 -eV range. Essentially, the same result is found in experiments involving electron⁴ and ion collisions.⁵ Since the energy resolution of the multiphoton data is not sufficient to exhibit the structure seen in the data produced in the x-ray studies, no significance can be attached to absence of those structured features in the multiquantum result. Overall, therefore, the gross character of the spectrum of the N^+ ions produced does not depend strongly on the

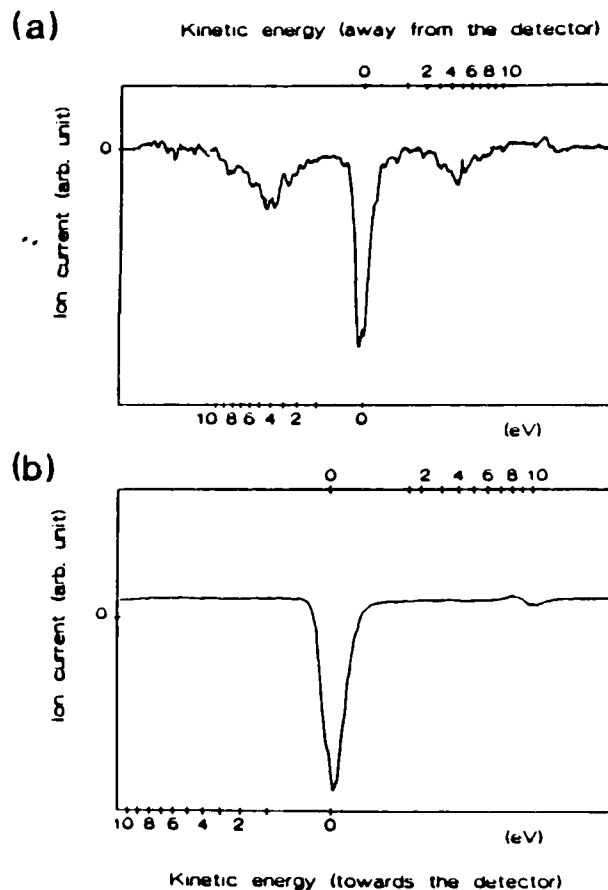


FIG. 1. (a) Time-of-flight N^+ -ion signal arising from multiphoton ionization of N_2 . The central feature arises from very-low-energy ions while the two symmetrically located components arise from energetic molecular dissociation from oppositely directed fragments of equal energy. See text for discussion. (b) Time-of-flight ion signal corresponding to N_2^+ , a species for which the dissociative components are absent. In this case only a single peak is seen corresponding to the thermal kinetic energy of the parent N_2 molecules.

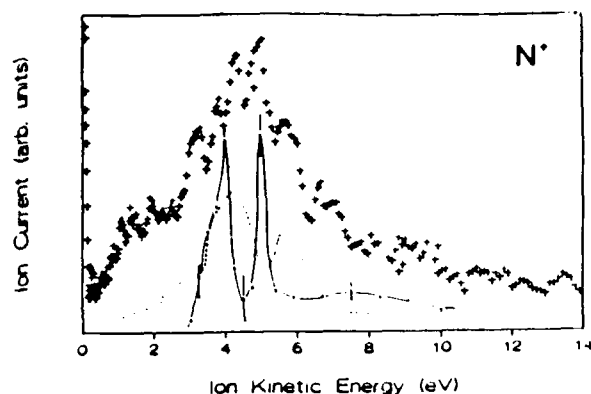


FIG. 2. Ion current (N^+) vs ion kinetic energy for N_2 . The + data arise from the multiphoton ionization at 248 nm. The solid curve (\circ) represents the results of Saito and Suzuki (Ref. 3). The dashed curve is taken from the results of Eberhardt, et al. (Ref. 1).

mechanism of ionization. X rays, electrons, ions, and multiphoton coupling all produce N^+ ions of approximately the same energy.

Ranked in order of ascending binding energy, the outer molecular orbitals of N_2 , based on the spectroscopy¹⁶⁻¹⁸ of N_2 and N_2^+ , are $1\pi_u$, $3\sigma_g$, $2\sigma_u$, and $2\sigma_g$, with values of ~ 15.6 , ~ 16.7 , ~ 18.7 , and ~ 38 eV, respectively. Consequently, these four orbitals represent two approximately separate scales of excitation with $1\pi_u$, $3\sigma_g$, and $2\sigma_u$ being the lowest, and $2\sigma_g$ the highest.

For the channel producing the N^+ ions observed, the N_2^{2+} valence holes leading to dissociation appear to be primarily of $^1\Delta_g[1\pi_u^{-2}]$ character,^{19,20} the lowest-energy two-hole configuration. Since the KVV Auger process associated with the x-ray excitation occurs on a time short compared to molecular nuclear motions, the internuclear separation r_0 of the nascent N_2^{2+} system is expected to be very near to that given by the $N_2 X^1\Sigma_g^+$ ground state ($r_0 = 1.098$ Å). Therefore, the agreement of the N^+ fragment energies suggests that the multiphoton transition occurs at an internuclear separation close to the same value of r_0 . Low-lying metastable states^{21,22} of N_2^{2+} are presumably also formed from the decay which could account for the N^+ generation in the energy range ~ 2 eV.

The dominance of the $1\pi_u^{-2}$ configuration of N_2^{2+} produced by the multiquantum process is not unexpected, since it represents a rather low ionization energy and can be reached either by a direct path from $N_2 X^1\Sigma_g^+$ or a sequential mechanism involving the stable electronically excited $N_2^+ A^2\Pi_u$ state which has a $1\pi_u$ hole. A sequential mechanism proceeding through the lowest ion level, $N_2^+ X^2\Sigma_g^+$, to a $1\pi_u^{-2}$ configuration is considered unlikely, since the $X^2\Sigma_g^+$ state has a $3\sigma_g$ hole.^{16,23} The change in the equilibrium internuclear separation of ~ 0.08 Å between the $N_2 X$ and $N_2^+ A$ states is sufficiently small to have a negligible effect on the observed kinetic energy distributions for the energy resolution used in these studies.

The production of N^{2+} ions can be considered in a similar light. In this case, the agreement represented in

Fig. 2 between the x-ray-produced and multiphoton-generated N^+ distributions does not occur with respect to the corresponding N^{2+} kinetic energy distributions, if it is assumed that the ions arise only from the



channel. The data illustrating this comparison, which includes a fiducial signal arising from Ar^{6+} , are shown in Fig. 3. Roughly, the x-ray and multiphoton data agree for energies above ~ 10 eV, but deviate significantly otherwise. A substantial component of the multiphoton-generated ion signal is shifted to a considerably lower energy. Indeed, a prominent peak in the N^{2+} spectrum stemming from the nonlinear coupling is present at 6–7 eV, an energy range well below the lower limit of the soft-x-ray-produced particles.

The maximum exhibited in the 6–7-eV range in Fig. 3 for the multiquantum-produced N^{2+} ions, however, is consistent with formation by the reaction



a channel that is associated with a major feature of the Auger spectrum² of N_2 corresponding to a two-hole binding energy in the vicinity of ~ 70 eV. Indeed, in that region, the only decay channel observed² was process (3) with a characteristic N^{2+} energy of 6.7 ± 1 eV. The N_2^{2+} states implicated,^{2,20} as noted in the x-ray studies,² are $^1\Sigma_g[2\sigma_g^{-1}, 3\sigma_g^{-1}]$, $^1\Sigma_u[2\sigma_g^{-1}, 2\sigma_u^{-1}]$, and $^1\Pi_u[2\sigma_g^{-1}, 1\pi_u^{-1}]$. Furthermore, in those studies, spin conservation requires fragmentation from those singlet-hole configurations to excited products. The likely final states are $N^{2+}(^2P^*) + N(^2D^*)$, $N^{2+}(^2P^*) + N(^2P^*)$, and $N^{2+}(^4P) + N(^4S^*)$. The multiphoton data are consistent with approximately equal participation of these three channels. Interestingly, in related studies²⁴ of fragmentation of N_2 conducted at a wavelength of ~ 600 nm, process (4) was suggested in order to account for the total

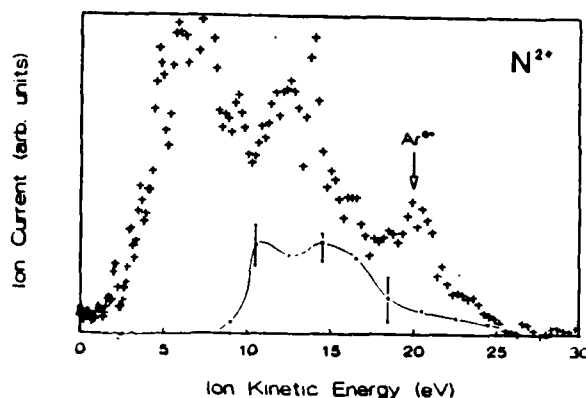


FIG. 3. Ion current (N^{2+}) vs ion kinetic energy for N_2 . The + data arise from the multiphoton ionization at 248 nm which includes, as a fiducial, a component at ~ 20 eV produced from Ar^{6+} . The solid (\circ) curve represents the data of Saito and Suzuki (Ref. 3) and corresponds only to the $N^{2+} + N^+$ channel. General agreement is seen except for the clear peak in the 6–7-eV region for the multiphoton data.

observed abundance of N_2^{2+} .

In parallel with the discussion of process (2) above, the N_2^{2+} system could be produced either by a direct mechanism from $N_2 X^1\Sigma_g^+$ or by a sequential mechanism involving states of N_2^+ . Since $N_2^+(X)$ and $N_2^+(A)$ have $3\sigma_g$ and $1\pi_u$ holes, respectively, the production of the $N_2^{2+} X^1\Sigma_g^+$ and the $N_2^{2+} B^2\Sigma_u^+$ levels given above could involve a sequential mechanism with X and A first-ion states serving as intermediate species. However, on the basis of the molecular configurations, the participation of the $1\Sigma_u[2\sigma_g^{-1}, 2\sigma_u^{-1}]$ state by a sequential process would not be expected to occur through the X and A states. Presumably, this would require the generation of significantly more highly excited N_2^+ levels, such as the $N_2^+ B^2\Sigma_u^+$ which involves a $2\sigma_u$ hole.

The neutral nitrogen atoms produced by process (4) would escape detection, but a fraction of them would be expected to be converted to N^+ after dissociation by subsequent multiphoton ionization in the focal zone. The presence of such a group of 6–7-eV N^+ ions would, therefore, contribute to the signal in that range shown in Fig. 2. Since the overall $[N^+]/[N_2^{2+}]$ ratio is significantly greater than unity, this component of the N^+ signal is expected to be relatively small in comparison to those produced by process (2).

Alternatively, since the high-energy region of the N^+ kinetic energy distribution overlaps the low-energy region of the N_2^{2+} distribution, the N_2^{2+} seen in the 6–7-eV range could, in principle, be produced entirely by a velocity-selective conversion by multiquantum ionization of N^+ to N_2^{2+} . Although the multiphoton data cannot rule out this possibility, the general agreement of the N^+ and N_2^{2+} distributions with the corresponding ones observed in the synchrotron studies diminishes the likelihood that such a selective conversion is playing a dominant role.

A distinct group of N_2^{2+} ions is apparent in Fig. 3 in the 11–14-eV region for both the multiquantum and synchrotron^{2,3} studies. The observation of N_2^{2+} with kinetic energies in the 11–14-eV range cannot plausibly be associated with channels in either N_2^+ or N_2^{2+} , even with allowance for a second step of ionization (e.g., $N^+ \rightarrow N_2^{2+}$) occurring after the act of molecular dissociation. The curves for these two species are simply not steep enough to give a sufficient impulse.^{16,19,20} A more highly charged system, presumably N_2^{3+} , which can undergo the reaction



is indicated. This, of course, is in agreement with the findings of the x-ray studies.³

For N_2^{3+} , the Coulomb term is expected to dominate the molecular curve, with the exception of relatively minor molecular contributions for internuclear separations in the ~ 1 -Å range. The Coulombic N_2^{3+} curve indicated in Fig. 4 shows that its position is consistent with the magnitude of the observed N_2^{2+} kinetic energies for an approximately vertical excitation of the system in the potential-energy region ~ 84 eV. Furthermore, within the experimental resolution (~ 3 eV), the 11–14-eV range agrees well with the observed N_2^{2+} energy (~ 13 eV) in the soft-x-ray studies² stemming, in that case, from N_2^{3+}

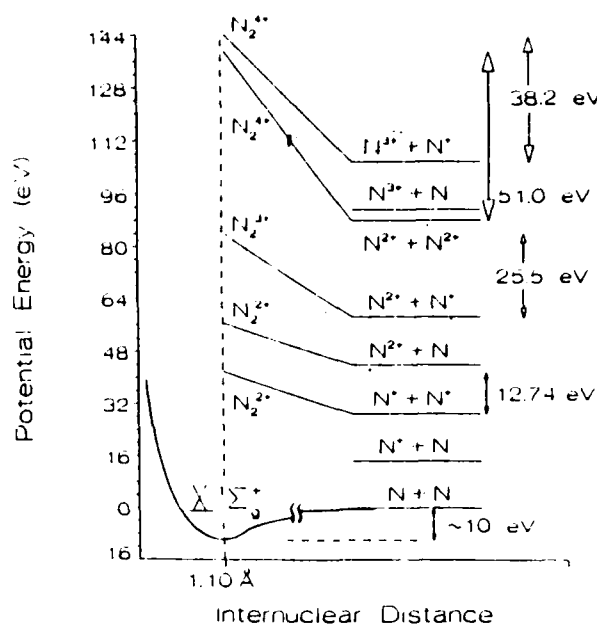
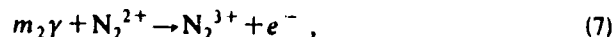
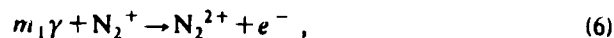


FIG. 4. A partial potential-energy diagram of N_2 indicating the ground $N_2 X^1\Sigma_g^+$ and the Coulombic contributions to several ionized species. Assuming vertical excitation, the ion energies observed will be one-half the amount indicated for the channels ($N^+ + N^+ \rightarrow 12.74$ eV; $N_2^+ + N_2^+ \rightarrow 25.5$ eV; $N_2^{3+} + N^+ \rightarrow 38.2$ eV). The $N_2^{2+} + N_2^{2+}$ (51.0 eV) was not observed. See text for discussion.

formation arising from a $2\sigma_g^{-2}$ level with the assumption of an additional shake-off from the first Auger event.

Overall, the observed N^+ and N_2^{2+} distributions, assuming that the ions arise from the decay channels $N^+ + N^+$, $N_2^+ + N$, and $N_2^{2+} + N^+$, all appear consistent with nearly vertical excitation of the N_2 system to corresponding N_2^{2+} and N_2^{3+} configurations. It is also known¹⁷ that the ionic ground and low-lying N_2^+ levels ($X^1\Sigma_g^+$, $A^2\Pi_u$, and $B^2\Sigma_u^+$) all have equilibrium internuclear separations very close to the neutral N_2 ground state $X^1\Sigma_g^+$. Therefore, the removal of one electron from the neutral molecule does not cause appreciable nuclear motion or displacement. Excitation to higher-charge states, however, such as N_2^{2+} and N_2^{3+} , generally leads to unstable levels which will cause rapid motion of the nuclei. Since N_2 and N_2^+ are stable with $r_{N_2} \approx r_{N_2^+}$ the present multiphoton data do not give information on the removal of the first electron. However, the observation of dissociative channels from N_2^{2+} and N_2^{3+} enables an estimate to be made concerning the dynamics of electron removal involving those systems.

Consider the production of N_2^{3+} from N_2^+ by the sequential mechanism



in which m_1 and m_2 denote the number of ultraviolet quanta involved. The observed absence of appreciable nuclear motion in the formation of N_2^{3+} can be used to estimate a residence time τ for the unstable N_2^{2+} system.

This gives an approximate figure for the electron emission rate for the physical regime being studied. For this estimate we will assume that the N_2^{3+} and N_2^{3+} molecular curves are dominated by the Coulombic interactions corresponding to $N^+ + N^+$ and $N^{2+} + N^+$, respectively. In this picture, the net change in the kinetic energy $\Delta\phi$ of the N^{2+} fragment produced by process (5) arising from a small displacement Δr in the N_2^{3+} ($N^+ + N^+$) system can be simply represented by

$$\Delta\phi = \frac{e^2}{r_0} - \frac{e^2}{r_0 + \Delta r}, \quad (8)$$

in which r_0 is the initial internuclear distance. The data indicate that

$$r_0 \approx r_{N_1} \approx r_{N_2} \approx 1.1 \text{ \AA}. \quad (9)$$

The magnitude of Δr can be derived from Eq. (8) by equating $\Delta\phi$ with the shift observed in the N^{2+} energies between the synchrotron data² and the multiphoton results arising from the $N^{2+} + N^+$ decay. Since no shift was observed, we use the experimental energy resolution $\Delta\epsilon$ of N^{2+} to establish an upper bound Δr_m on this displacement. The result is

$$\Delta r_m \leq r_0 \left[\frac{1}{(e^2/r_0\Delta\epsilon) - 1} \right] \quad (10)$$

which, with $\Delta\epsilon \approx 3$ eV, gives $\Delta r_m \leq 0.33 \text{ \AA}$. The corresponding upper bound on the residence time τ_m of the N_2^{3+} system can be evaluated from Eq. (1) with $Z_1 = Z_2 = 1$, the parameter β selected so that

$$2\beta a_0 = r_0, \quad (11)$$

and

$$x = r_0 + \Delta r_m. \quad (12)$$

This gives $\beta \approx 1.04$, $x \approx 1.43 \text{ \AA}$, and yields

$$\tau_m \approx 2.35 \text{ fs}, \quad (13)$$

an interval that is only three periods of the 248-nm wave. Therefore, the ion energy distributions indicate that the lifetime of the N_2^{2+} species, as an intermediary in the production of N_2^{3+} from lower charge states (N_2 or N_2^+), is on the order of or less than approximately three cycles of the wave.

A substantial signal of N^{3+} ions was detected with the peak in the distribution occurring at ~ 20 eV as shown in Fig. 5. If we assume that the channel producing these ions is



and further assume that the ionization occurs at the internuclear separation implied by the production of the N^+ and N^{2+} species, the energy of the N^{3+} fragment would be exactly $\frac{1}{2}$ -fold the energy of the N^{2+} ion produced in the $N^{2+} + N^+$ reaction. Given the peak at ~ 12.8 eV for N^{2+} shown in Fig. 3, the expected N^{3+} kinetic energy is ~ 19.1 eV, a value very close to the measured maximum of the distribution at ~ 20 eV and indis-

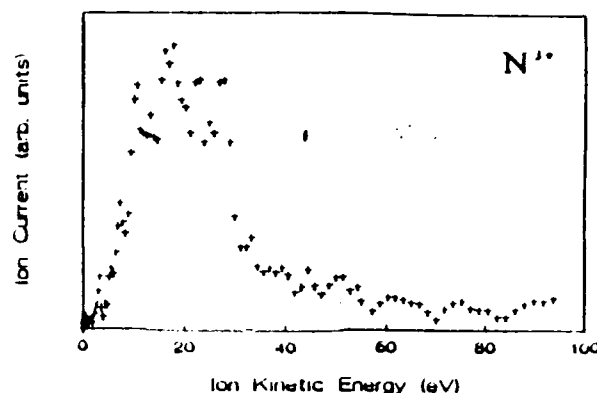


FIG. 5. Ion current (N^{3+}) vs ion kinetic energy for multiphoton ionization of N_2 at 248 nm. A prominent component exists in the 19–20-eV region.

tinguishable from it with the experimental resolution pertaining to this measurement.

We note that the N^+ component arising from reaction (14) is expected to be difficult to observe. The fraction of N^+ ions produced in that way is relatively small and any conversion of N^+ to N^{2+} by subsequent ionization would be effectively masked by the Ar^{6+} fiducial signal at ~ 20 eV.

Finally, if N_2^{3+} is regarded as an intermediate in the formation of N_2^{4+} , in parallel with the discussion above concerning N^{2+} -ion production following the formation of N_2^{3+} , a maximum residence time roughly comparable to that found for N_2^{2+} in Eq. (13) is found to apply.

Similar reasoning concerning the generation of N^{2+} ions from the N_2^{4+} system would place the corresponding N^{2+} energy at ~ 25 eV, a point for which no signal is evident in the distribution illustrated in Fig. 3. Apparently, the



channel is not dynamically favored under the conditions studied in this work, although clearly energetically accessible, since the $N^{2+} + N^{2+}$ potential lies in Fig. 4 below the corresponding $N^{3+} + N^+$ curve for all values of internuclear separation $r \geq r_0$. Interestingly, reaction (15) has been detected in other studies using covariance mapping²⁴ conducted under different conditions of frequency, maximum intensity, and pulsewidth. One was performed at $\sim 3 \times 10^{15} \text{ W/cm}^2$ at ~ 600 nm with 0.6-ps pulses²⁴ while another was conducted at $\sim 2 \times 10^{15} \text{ W/cm}^2$ at 248 nm with ~ 5 -ps pulses.²⁵ The values of these intensities represent peak magnitudes achieved in the focus, whereas the intensity of $\sim 10^{16} \text{ W/cm}^2$ pertaining to our experiments was determined by averaging over the central Airy disk. In addition, their findings²⁴ indicate that the molecular transitions tend to progress in a rather less vertical fashion. Although not strictly applying to the regime studied, the Keldysh formulation indicates that either lower frequency or lower intensity would reduce the transition rate. Given this tendency, and because the cited experiments^{24,25} have either one or both, it is not surprising that the ionization occurs at a somewhat

greater internuclear separation. These results point to sensitivities of the multiphoton amplitudes with respect to frequency, intensity, and pulse width which require further examination in future work.

IV. CONCLUSIONS

The kinetic energy distributions of atomic nitrogen ions produced from N_2 by multiphoton ionization reveal several characteristics of the nonlinear molecular interaction. In comparison to soft-x-ray excitation, which produces the molecular vacancies by Auger cascade and shake-off, the final configurations of the valence-shell holes produced by the multiphoton and soft-x-ray excitation appear to have many similarities.

The observed kinetic-energy distributions of the N^+ , N^{2+} , and N^{3+} ions produced by the multiphoton mechanism all find consistent explanation if it is assumed that the molecular ionization for all species occurs at an internuclear separation close to the equilibrium value for neutral N_2 . Namely, the transitions appear to occur nearly vertically. This finding enables an estimate of the effective residence time of intermediate molecular ionic states to be made with the outcome that this interval has an upper bound on the order of a few optical cycles for N_2^{2+} and N_2^{3+} . Since most of the deposited energy is associated with the formation of the higher-charge states, the implication is that the main energy-transfer process, when it occurs in the course of the interaction, proceeds quite rapidly. A peak energy-transfer rate on the order of a few milliwatts per molecule is inferred from these results. Therefore, a mechanism for strong coupling is presumably present.

Four molecular decay modes are identified involving molecular-ion states with a charge as high as N_2^{4+} . They are, specifically, $N^+ + N^+$, $N + N^{2+}$, $N^+ + N^{2+}$, and $N^+ + N^{3+}$. It is notable that three of these represent charge asymmetric modes and that an energetically available symmetric decay channel ($N^{2+} + N^{2+}$) was apparently not present at a detectable level. The dynamics appear to favor asymmetric channels. We observe that the enhancement of an asymmetric mode, such as $N + N^{2+}$, is a mechanism tending to cause an increase in

the $[N^{2+}]/[N^+]$ fraction, a noted feature of the multiphoton data with respect to comparison with the yields observed in the synchrotron studies.

A simple hypothesis unites the rapid energy transfer, leading to vertical molecular transitions with the observed tendency to produce charge asymmetric dissociation. The presence of a large induced dipole arising from a multielectron motion will enhance the ability of the N_2 system to couple to the field. Such a dipole, however, represents a large asymmetric displacement of charge, a situation that would naturally lead to a corresponding asymmetry in the charge states of the dissociation products. This effect would be expected to be most significant for a situation involving a parallel orientation of the molecular axis along the electric vector of the ultraviolet wave.⁷ In this sense, the observed charge asymmetry of the ionic products is merely a remnant of the induced electronic motions. Interestingly, the driven excursion of a free electron at $\sim 10^{16}$ W/cm² in a 248-nm field is ~ 8.4 Å, a value more than 7 times larger than the equilibrium internuclear separation of N_2 . Even with a considerable reduction of the scale of this motion arising from the restoring binding forces in the molecule, a substantial charge displacement of the outer molecular electrons is expected under these conditions. A system behaving in this way does not decide its fate on the basis of the energy scale associated with potential final states, but rather selects the dynamical mode of interaction which favors the strongest coupling. Hints of similar behavior were seen in earlier studies of the atomic number dependence of multiphoton ionization of atoms.²⁶ Consequently, the final states to which such electronic motions are related become prominent in the observed distributions of the ionic products.

ACKNOWLEDGMENTS

The authors acknowledge fruitful discussions with G. Wendin. This work was supported by the U. S. Office of Naval Research, the U. S. Air Force Office of Scientific Research, the Directed Energy Office and the Innovative Science and Technology Office of the Strategic Defense Initiative Organization, and the National Science Foundation.

*Present address: Theoretical Division MS-B210, Los Alamos National Laboratory, Los Alamos, NM 87545.

¹W. Eberhardt, J. Stöhr, J. Feldhaus, E. W. Plummer, and F. Sette, *Phys. Rev. Lett.* **51**, 2370 (1983).

²W. Eberhardt, E. W. Plummer, I.-W. Lyo, R. Carr, and W. K. Ford, *Phys. Rev. Lett.* **58**, 207 (1987).

³Norio Saito and Isao H. Suzuki, *Phys. B* **20**, L785 (1987).

⁴B. Brehm and G. deFrenes, *Int. J. Mass Spectrom. Ion Phys.* **26**, 251 (1978).

⁵A. K. Edwards and R. M. Wood, *J. Chem. Phys.* **76**, 2938 (1982).

⁶F. J. Frasniski, K. Codling, P. Hatherly, J. Barr, I. N. Ross, and W. T. Toner, *Phys. Rev. Lett.* **58**, 2424 (1987).

⁷K. Codling, L. J. Frasniski, P. Hatherly, and J. R. M. Barr, *J. Phys. B* **20**, L525 (1987).

⁸C. K. Rhodes, in *Ordered Many-Electron Motions in Atoms and X-Ray Lasers*, Proceedings of the NATO Advanced Study Institute on Giant Resonances in Atoms, Molecules, and Solids, edited by J. P. Connerade, J. M. Esteve, and R. C. Karnatak (Plenum, New York, 1987) p. 533.

⁹T. A. Carlson and M. O. Krause, *J. Chem. Phys.* **56**, 3206 (1972).

¹⁰T. A. Carlson and R. M. White, *J. Chem. Phys.* **44**, 4510 (1966).

¹¹A. P. Schwarzenbach, T. S. Luk, I. A. McIntyre, U. Johann, A. McPherson, K. Boyer, and C. K. Rhodes, *Opt. Lett.* **11**, 499 (1986).

¹²W. C. Wiley and I. H. McLaren, *Rev. Sci. Instrum.* **26**, 1150 (1955).

¹³T. S. Luk, U. Johann, H. Egger, H. Plummer, and C. K.

- Rhodes, Phys. Rev. A 32, 214 (1985).
- ¹⁴T. S. Luk and C. K. Rhodes, Phys. Rev. A 38, 6180 (1988).
- ¹⁵W. Eberhardt, E. W. Plummer, C. T. Chen, R. Carr, and W. K. Ford, Nucl. Instrum. Methods A 246, 825 (1986).
- ¹⁶A. Lofthus, J. Phys. Chem. 6, 113 (1977).
- ¹⁷K. P. Huber and G. Herzberg, *Constants of Diatomic Molecules* (Van Nostrand Reinhold, New York, 1979).
- ¹⁸J. L. Gardner and James A. R. Samson, J. Chem. Phys. 62, 1447 (1975).
- ¹⁹E. W. Thulstrup and A. Anderson, J. Phys. B 8, 965 (1975).
- ²⁰H. Ågren, J. Chem. Phys. 75, 1267 (1981).
- ²¹L. Hellner, M. J. Besnard, G. Dujardin, and Y. Malinovich, Chem. Phys. 119, 391 (1988).
- ²²R. W. Wetmore and R. K. Boyd, J. Phys. Chem. 90, 5540 (1986).
- ²³W. E. Moddeman, T. A. Carlson, M. D. Krause, B. P. Pullen, W. E. Bull, and G. K. Schweitzer, J. Chem. Phys. 55, 2317 (1971).
- ²⁴F. J. Frasiniski, K. Codling, and P. A. Hatherly (unpublished).
- ²⁵K. Codling (private communication).
- ²⁶T. S. Luk, H. Pummer, K. Boyer, M. Shahidi, H. Egger, and C. K. Rhodes, Phys. Rev. Lett. 51, 110 (1983).